4

Asymmetry induced rippling in mixed surfactant bilayers from dual-scale simulations

4.1 INTRODUCTION

Surfactant molecules can self-assemble into a wide range of topologically distinct lamellar phases such as gel, interdigitated gel, tilted gel, ripple and liquid crystalline phases [Israelachvili *et al.*, 1977; Shang *et al.*, 2006; Debnath *et al.*, 2009; Lunkad *et al.*, 2017]. Understanding the origin of these distinct phases is important to design phases with desired functionality relevant for industrial or biological applications. The ratio of head group to chain length of surfactants can create a difference in packing resulting in formation of micelles, lamellar phases and so on [Israelachvili *et al.*, 1977]. Compositions, pressure, hydration and temperature are few known parameters responsible for gel to tilted gel to ripple to fluid lamellar phase transitions [Debnath *et al.*, 2014; Takeda *et al.*, 2019]. Among these phases, fluid phases are extensively studied since they resemble naturally existing cell membranes [Elson *et al.*, 2010; Kucerka *et al.*, 2005].

In comparison to the fluid phases, the gel phases are less investigated. Gel phases have biological significance for specific cases such as stratum corneum [Bouwstra *et al.*, 1992]. Recent studies using molecular biology reveal evidences of functionally relevant gel like sterol free rafts in living cells [Vecer *et al.*, 2014; Aresta-Branco *et al.*, 2011]. Gel phases are routinely used for cosmetic formulations and topical treatments since they retain moisture with improved barrier properties [Yang *et al.*, 2020]. Lamellar gel phases are key components of hair conditioners that provide better wet conditions by optimized performance with respect to the rheological properties, stability etc. [Davies and Amin, 2020]. Moreover, structures of model membranes in the gel phase build the foundation for preparation of fluid phases and thus is of general interest [Tristram-Nagle *et al.*, 2002; Sun *et al.*, 1996; Katsaras *et al.*, 2000]. Molecular dynamics simulations of PE lipids using Berger and CHARMM36 force-fields show that initial alignment of glycerol backbone influences the resulting structure of the bilayer at gel phase [Uppulury *et al.*, 2015]. Binary and ternary mixtures of DPPC, DPPE and cholesterol have been simulated using all atom molecular dynamics simulations. Co-existences of L_α and gel or ripple phases and L_o and L_d or gel phases have been found for the binary and ternary mixtures respectively [Gu *et al.*, 2020]. The co-existence of gel and fluid like domains in bilayers facilitates pore mediated ionic permeability at the constriction region [Cordeiro, 2018].

Similar to the gel phase, ripple phases are less attended so far. A liquid crystalline phase of lecithin bilayer spontaneously produces ripple phase ($P_{\beta'}$) using all atom molecular dynamics simulations once temperature is decreased [de Vries *et al.*, 2005]. The $P_{\beta'}$ phase consists of a gel like non-interdigitated major domain and fully interdigitated ($L_{\beta I}$) minor domain. A ripple phase has been identified for DMPC bilayers using small angle X-ray scattering experiments where the major arm is in $L_{\beta F}$ gel state and the minor arm is in a disordered state [Akabori and Nagle, 2015]. A statistical mechanical model predicts that attractive van der Waals forces and larger head groups to hinder level packing are two essential features for the ripple phase of lecithin bilayers [Pearce and Scott, 1982b]. Head-head repulsion parameter and tail length are identified as two key parameters to obtain a ripple phase in a mesoscopic model [Kranenburg and Smit, 2005]. Dissipative-particle dynamics shows formations of ripple phases where computational calorimetric method is introduced to measure enthalpy of saturated lipids [Rodgers *et al.*, 2012]. Earlier a

theoretical model predicts that the chain tilt can induce instabilities in a flat phase and break the inversion symmetry which is also observed by the experimental studies [Seifert *et al.*, 1996]. A generic model with larger head group size can generate a ripple phase between a tilted gel phase ($L_{\beta'}$) and a L_α phase. A reduction in the head group size results in an untilted gel phase which subsequently does not reproduce a ripple phase [Düchs and Schmid, 2001; Lenz and Schmid, 2005, 2007; Schmid *et al.*, 2007]. MARTINI coarse-grained model typically does not reproduce tilted gel phase for saturated phospholipids without advanced sampling and thus is not known to generate the ripple phase [Schmid *et al.*, 2014]. Theoretically ripple phases can be obtained from a local phase separation between gel and liquid phase and a curvature stress generally in the ordered state resulting from head to tail size mismatch.

Two dimensional (2D) ripple, known as the square phase, are rarely found. A continuum Landau theory predicts that a coupling between curvature and tangent plane orientational order results in 2D ripple phases [Chen *et al.*, 1995]. Similar to the predicted model, a square modulated phase of phospholipids is observed using x-ray diffraction study from the liquid crystalline phase by dehydration or cooling [Yang and Fukuto, 2005]. DPPC bilayers are found to develop square like phases using freeze-fracture electron microscopy and x-ray diffraction when 5-10 mol % sterols are added [Meyert *et al.*, 1997]. Such a small fraction of literature on experimental evidence of these phases certainly show that a general principle or method to achieve these phases are lacking.

The complex micro-organization of the ripple phase makes it an interesting system of study for understanding of lipid order-disorder transition in a broader perspective. However, research on gel and ripple phases are less attended so far due to their poorly understood relevance to biological systems unlike the fluid phase. Moreover, very limited literature is available on gel or ripple phases comprised of surfactants immensely used in cosmetic formulations, detergents, oil recovery processes and so on. Reproducing ripple phases with desired dimensionality is particularly challenging since the phase exists near gel to liquid crystalline phase transition and a small variation in the parameter space can make the phase quickly disappear. Thus we attempt to obtain molecular insights on the structure and stability of the gel and ripple phases using molecular dynamics simulations. Implications of our current work are two-fold: a) tunable physical parameters can be obtained for a desired topology of aggregated surfactant molecules relevant for industrial applications, b) current understanding on lateral organizations of the ripple and gel phase can be applied on nano-domain formations in multi-component biological membranes due to similar physical behavior of surfactants as lipid molecules.

Mixed surfactant molecules from random configurations are spontaneously self-assembled into bilayers which are found to be asymmetric in terms of populations across two leaflets. Asymmetry is a key feature in naturally existing cell membranes [Tian *et al.*, 2016; Kiessling *et al.*, 2006] and can change the phase behavior of inner vs outer leaflet which may lead to different thermodynamical characteristics [Perlmutter and Sachs, 2011]. Although recent experiments are successful in creating well controlled artificial asymmetric model membranes [Doktorova *et al.*, 2018], influence of trans-leaflet asymmetry on the ripple phase has not been investigated at the molecular level yet. Moreover, the time and length scales relevant for examining the stability of a membrane at gel or ripple phase cannot be achieved solely using an AA model due to its very slow dynamics. Since the well known MARTINI force-field does not provide the bonded potentials for the mixed surfactant molecules used in this study and does not typically reproduce the ripple phase, a mixed approach of independent bonded and non-bonded potentials in deriving a CG model has been followed. In doing so, we examine if mixed surfactant systems can be coarse-grained following similar assumptions as for a single component system. The methodology followed to coarse grain the systems studied here is well established for lipid bilayers, polymers, liquid crystals, proteins in membranes and so on [Bezkorovaynaya *et al.*, 2012; Debnath *et al.*, 2015]. Bonded and non-bonded distributions are calculated for bilayers at both AA and CG scales and compared with each other. Asymmetry percentage, extent of interdigitation, tilt and order parameter are calculated to understand the lateral structure of gel and ripple phases. Configurational entropy per chain is

calculated for bilayers of both resolutions to find out the thermodynamics and molecular origin of the asymmetry. The present investigation focuses on: 1) the influence of trans-bilayer asymmetry on inducing gel or ripple phases in mixed surfactant bilayers, 2) interplay of entropy per chain, tilt and order parameter across two layers and their effects on the lateral organization of the lamellar phase, 3) relations between thermodynamical and physical properties of the gel/ripple lamellar phase. Our analyses can be extended towards understanding the thermodynamics of molecular asymmetry relevant for ordered-disordered domain formations and associated transport in membranes in the future.

4.2 COMPUTATIONAL DETAILS

4.2.1 Atomistic simulation details

Seven sets of AA simulations are carried out for systems composed of a cationic surfactant, BTMAC and a co-surfactant, SA in presence of SPC water [Pekka and Lennart, 2001] at 283 K at a BTMAC to SA ratio of 2 : 1 by varying initial configurations. This specific composition results in formation of a lamellar phase [Lunkad *et al.*, 2017]. The chemical formula of a BTMAC and a SA molecule are shown in figure 2.1. The force-fields of BTMAC and SA are obtained from Gromos-87 [van Gunsteren and Berendsen, 1987] and OPLS-AA [Jorgensen, 1986; Kaminski *et al.*, 2001] and the parameters are reported in table 2.1. Using these force-fields of BTMAC and SA, in combination with SPC water model the gel to liquid crystalline phase transition temperature obtained from experiment is correctly reproduced and reported earlier [Debnath *et al.*, 2009].

In the present work, bilayers S1 to S8 are investigated using the same force-field and details of the systems studied are described in table 4.1 in the decreasing order of their compositional asymmetry. The differences in the number of surfactant molecules across two layers are referred to as asymmetry in our study. The initial configurations of S1 and S8 are prepared from asymmetric bilayers and the initial configurations of S5 is a symmetric bilayer. These configurations are generated using Packmol v18.169 [Martínez *et al.*, 2009; Martínez and Martínez, 2003]. The objective of creating such biased starting configurations for these cases is to check if homogeneous distributions of mixed surfactant molecules in a symmetric bilayer generate any height modulations for the composition investigated. The starting configurations of other 4 systems (S2, S3, S4 and S7 in table 4.1) are varied either by random initial positions or velocities to investigate if the self-assembled bilayers lead to uniform or non-uniform mixing across leaflets. Systems S2 and S4 differ only in random initial positions and systems S3 and S7 differ in random velocities in addition to random initial positions to generate different initial conditions for the simulations. The number of molecules of BTMAC and SA are reported in table 4.1. To maintain electro-neutrality, chloride ions are added to each system where the number of chloride ions is equal to the number of BTMAC molecules. For all cases, the initial configurations are energy minimized using steepest descent algorithm [Leach, 2001]. NVT simulations of 100 ps are performed at 283 K using velocity rescale method [Bussi *et al.*, 2007a] with a temperature coupling constant of 0.5 ps. Next, all systems are simulated in a constant pressure of 1 atm using Berendsen semi-isotropic pressure coupling method [Berendsen *et al.*, 1984].

The surfactants in systems S2, S3, S4, S7 spontaneously self-assemble into asymmetric double bilayers where the box-lengths along the bilayer normals and along their perpendicular directions turn out to be the same and the other box-lengths are shorter. Single bilayer out of the double bilayers is extracted as both bilayers are equivalent for each of these cases. The shorter box-length is replicated four times to keep it close to the other box-length. This results in unequal box-lengths encompassing the bilayer surface although the semi-isotropic pressure coupling is used. Since S8 is a biased system created using Packmol to have the same asymmetry percentage as in S7, the box-lengths of S8 are kept similar to S7. All systems are simulated for $100 - 300$ ns with

Table 4.1: Compositions, initial and final configurations, run-lengths and asymmetry percentage of systems investigated. The asymmetry in each system is computed using equation 4.1. The asymmetry percentage remains unchanged from AA to CG scales except S5 which has a standard deviation of 0.77% in asymmetry.

Model	System	Initial configuration	No. of molecules BTMAC/SA	Water	NPT (ns)	Final bilayer	Asymmetry %
AA	S1 (Maximum (asymmetry)	Asymmetric bilayer	400/200	19800	120	Asymmetric 2D ripple	27.6
	S2 (Maximum asymmetry)	Random position	800/400	39600	100	Asymmetric 1D ripple	27.6
	S3	Random velocity	800/400	39600	120	Asymmetric 2D ripple	15.7
	S4	Random position	800/400	39600	120	Asymmetric interdigitated gel	13.92
	S5 (Intermediate asymmetry)	Symmetric bilayer	400/200	19800	200	Asymmetric 2D ripple	12.06 ±0.77
	S7 (Minimum Asymmetry)	Random velocity	800/400	39600	120	Asymmetric interdigitated gel	2.99
	S8 (Minimum asymmetry)	Asymmetric bilayer	800/400	39600	400	Asymmetric interdigitated gel	2.66
CG	S1 (Maximum asymmetry)	Asymmetric 2D ripple	400/200	4950	5500	Asymmetric 2D ripple	27.6
	S2 (Maximum asymmetry)	Asymmetric 1D ripple	800/400	9900	5500	Asymmetric 1D ripple	27.6
	S3	Asymmetric 2D ripple	800/400	9900	5500	Asymmetric 2D ripple	15.7
	S4	Asymmetric	800/400	9900	5500	Asymmetric interdigitated gel	13.92
	S5 (Intermediate asymmetry)	Asymmetric 2D ripple	400/200	4950	5500	Asymmetric 2D ripple	12.5
	S6 (Intermediate asymmetry) (larger system)	Asymmetric 2D ripple	3600/1800	44550	5200	Asymmetric 2D ripple	12.5
	S7 (Minimum asymmetry)	Asymmetric	800/400	9900	5500	Asymmetric interdigitated gel	2.99
	S8 (Minimum asymmetry)	Asymmetric	800/400	9900	6000	Asymmetric interdigitated gel	2.66

a time step of 2 fs. Coulombic interactions are treated with Particle Mesh Ewald method [Ewald, 1921] with a grid size of 0.12 nm. Interestingly final configurations of S1, S3 and S5 are asymmetric 2D rippled bilayers, S2 is a 1D rippled bilayer. S1 and S8 remain asymmetric. The NPT run lengths and the nature of the final configurations for all equilibrated systems are summarized in table 4.1. Equilibration of all systems are examined based on the convergence of area per surfactant head (APS), solvent accessible surface area (SASA) (figure 4.1) and the time evolution of per chain configurational entropy which is discussed later. Area per surfactant molecule (APS) obtained for all systems (table 4.2) shows that our systems reach APS comparable to the ones simulated earlier at both levels of resolutions. Volume per surfactant (VPS) are computed for all systems as products of APS and average chain lengths (shown in table 4.2). The system sizes of all final configurations of the bilayers obtained from AA simulations are reported in table A1 in the appendix.

Since the bilayers are self-assembled spontaneously for most of the cases, asymmetry is not created in a controlled manner in our simulations. The percentages of asymmetry and the final configurations for all the systems studied are mentioned in table 4.1. As asymmetry percentages vary from S1-S8, the SASA, APS and per chain configurational entropy reach convergence at different

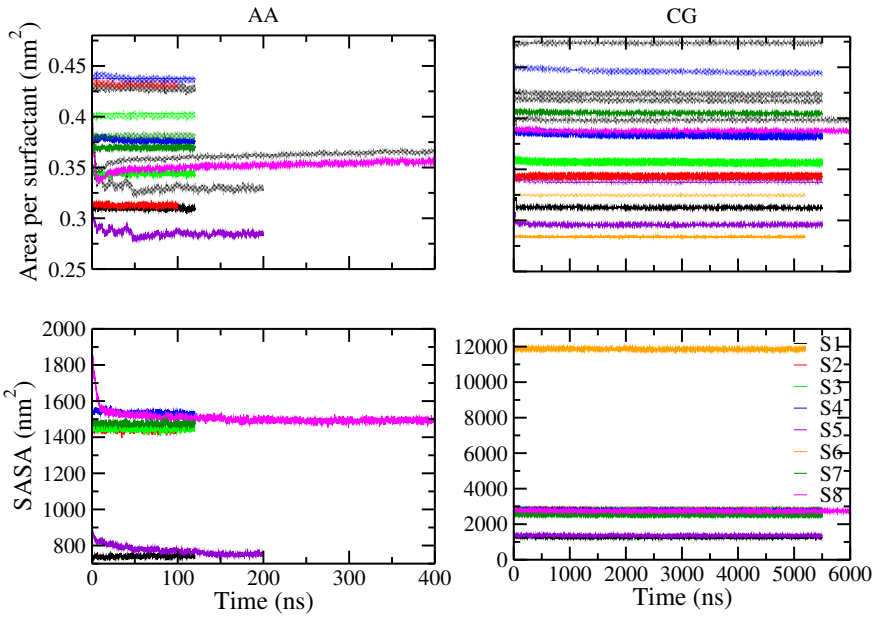

Figure 4.1: Area per surfactant (APS) and solvent accessible surface area (SASA) for all systems at AA and CG resolutions. The AA simulation of S8 has longer run than other systems since its per chain configurational entropy of the surfactants did not converge well until 400 ns. Similarly, the CG S8 system is simulated for 6 μs so that the SASA and APS of the system are well converged.

Table 4.2: Area per surfactant molecule (APS) (nm^2) and volume per surfactant (VPS) (nm^3) of simulated bilayers at AA and CG resolutions. M_p and L_p denoted the more and the less populated leaflets respectively. Standard deviations of APS at AA and CG resolutions are 0.001 and 0.0002-0.0003 respectively. [a][Lunkad *et al.*, 2017], [b][N Stelter and Keyes, 2017], [c][Boek *et al.*, 2005a].

System	APS AA			APS CG			VPS	
	M_p	L_p	Average	M_p	L_p	Average	AA	CG
S1 (Maximum asymmetry)	0.31	0.43	0.37	0.31	0.39	0.35	0.82	0.77
S2 (Maximum asymmetry)	0.31	0.43	0.37	0.34	0.47	0.41	0.83	0.89
S3	0.34	0.40	0.37	0.36	0.42	0.39	0.82	0.86
S4	0.38	0.44	0.41	0.38	0.44	0.41	0.91	0.91
S5 (Intermediate asymmetry)	0.28	0.33	0.31	0.29	0.34	0.32	0.70	0.70
S6 (Intermediate asymmetry)	-	-	-	0.28	0.32	0.30	-	0.66
S7 (Minimum asymmetry)	0.37	0.38	0.36	0.41	0.42	0.41	0.81	0.91
S8 (Minimum asymmetry)	0.35	0.36	0.36	0.39	0.40	0.39	0.81	0.85
Simulation results from literature	Surfactant-cosurfactant, BTMAC-SA (gel), ~0.38[a] Anionic surfactant, Erucate-128 (gel), 0.26[c]			Lipid, DPPC (gel), 0.50[b] Anionic surfactant, Erucate-128 (gel), 0.29[c]				

time resulting in different equilibration run-lengths for different systems. All the simulations have been carried out using GROMACSv4.6.5 [Bekker *et al.*, 1993; Abraham *et al.*, 2018; Lindahl *et al.*, 2001; Berendsen *et al.*, 1995; van der Spoel *et al.*, 2005; Hess *et al.*, 2008; Pronk *et al.*, 2013; Páll *et al.*, 2015; Abraham *et al.*, 2015]. All AA analyses are performed for the last 50 ns production runs based on the convergence of per chain configurational entropy of both the surfactants.

Previous studies of BTMAC/SA/water systems using all-atom simulations show different phases depending upon the bilayer composition. Variations of BTMAC to SA ratio from 1:2 to 3:5 to 2:3 at 283 K show gel to 1D rippled to 2D rippled phase transitions respectively, where the 2D rippled bilayer changes to gel phase upon heating [Debnath *et al.*, 2014]. Hence, to probe the effect of temperature on the stability of rippled asymmetric bilayers obtained from our simulations, the final configurations of bilayers S1 (maximum asymmetry), S5 (intermediate asymmetry) and S8 (minimum asymmetry) are at heated to 308 K with a scan rate of 2 K/ns. Similar scan rate has been followed to study the phase transition of a DPPC bilayer using all-atom simulation [Sun and Bckmann, 2017]. These bilayers are further simulated in the NVT ensemble for 500 ps and equilibrated for 10 ns in the NPT ensemble with similar parameters mentioned previously. Next, they are cooled back to 283 K with the same scan rate followed by NVT and NPT simulations.

4.2.2 Coarse-grained Simulations

Mapping scheme, bonded and non-bonded potentials

The initial CG configuration is obtained from the final configurations of the respective AA simulations in all the systems mentioned in table 4.1. AA BTMAC and SA are mapped into CG representation using VOTCA [Rühle *et al.*, 2009] following the same 4:1 mapping scheme of MARTINI as discussed in the previous chapter [Marrink *et al.*, 2007]. The mapped CG configurations of BTMAC and SA are shown in figure 3.1. CG bonded potentials are obtained by the Boltzmann inversion of the respective atomistic distribution (discussed in the previous chapter) and non-bonded interactions are treated with the MARTINI force-field.

Simulation details

Initial configuration of each CG system is obtained from the direct mapping of final configuration of the equilibrated AA run. This results in similar CG box-lengths as the AA ones. The energy minimized of the CG systems is carried out using steepest descent algorithm which is followed by 100 ps simulations in NVT ensembles. The temperature is coupled at 283 K using v-rescale [Bussi *et al.*, 2007a] thermostat. Next, the systems are simulated in an NPT ensemble for 5.2-6 μs using time steps of 4-10 fs. Berendsen barostat is used to keep the pressure constant at 1 atm with a semi-isotropic pressure coupling in all the systems using a coupling constant of 3.0 ps. The electrostatic and van der Waals interactions are cut-off at 1.2 nm. In addition to the existing asymmetric bilayers, a larger CG bilayer S6 is also simulated to probe the effect of system size (table 4.1). The simulation run-lengths, final configuration of the systems and their asymmetry % are reported in table 4.1. The equilibration of the simulations is monitored by the evolution in SASA and APS with respect to time (shown in figure 4.1). The average APS and box lengths at CG levels are reported in table 4.2 and table A1 in the appendix respectively. All systems remain asymmetric for entire CG run-lengths and entropy is analyzed for last 5 μs. The production run lengths for all further calculations of CG asymmetric bilayers are based on the convergence of per chain configurational entropy which range from last 800 ns to 2.5 μs.

4.3 ANALYSIS

Asymmetry

Asymmetry is commonly understood as the difference in chemical compositions across two leaflets in a bilayer. For our systems, asymmetry is defined as the differences in populations of surfactant molecules across two layers in a bilayer. Asymmetry, λ, is calculated using the following equation,

$$\lambda = \frac{n_m - n_l}{n_m} \times 100 \tag{4.1}$$

where n_m and n_l are the total number of BTMAC and SA heads in more and less populated layers, respectively.

Extent of interdigitation

The extent of interdigitation of surfactant tails of opposing monolayers of a bilayer is determined by chain overlap parameter, $O_{overlap}$, given as

$$O_{overlap} = \frac{2L_a - d(x,y)}{L_a} \tag{4.2}$$

Here L_a is the time and ensemble average chain length of BTMAC and SA along the bilayer normal given by,

$$L_a = | < z_h > - < z_e > |. \tag{4.3}$$

z_h and z_e are the z coordinates of head and end beads respectively, angular bracket denotes the ensemble average. $d(x,y)$ is the bilayer thickness computed from the head to head distances between two layers. The bilayer thickness is computed using the equation,

$$d(x,y) = z_L(x,y) - z_M(x,y) \tag{4.4}$$

where $z_L(x,y)$ and $z_M(x,y)$ are the z co-ordinates of the heads of the less and more populated leaflets respectively as a function of the bilayer surface. Assuming from full interdigitation to no interdigitation, t_{ch} can range from $L_a < t_{ch} < 2L_a$. This is because the bilayer thickness can never be shorter than the chain lengths projected on the bilayer normal and can not be larger than the sum of the average chain lengths of two layers.

Per chain configurational entropy

To understand the molecular and thermodynamical origin of asymmetry in the bilayer, configurational entropy per chain is calculated following Schlitter formula [Schlitter, 1993],

$$S_{conf}^{per-chain} = \frac{k_B}{2} ln\ det(1 + \frac{k_B T e^2}{\hbar^2} M^{\frac{1}{2}} C M^{\frac{1}{2}}) > S_{true} \tag{4.5}$$

where e is Euler's number, T denotes the absolute temperature, k_B is the Boltzmann constant $\hbar$ is Planck's constant divided by 2π, M is 3N-dimensional diagonal matrix which has the masses of the particles and C is the covariance matrix during particle fluctuations, given as

$$C =< (x - < x >)(x - < x >)^T > . \tag{4.6}$$

x is the 3N-dimensional vector representing the coordinates of N particles for which the entropy has to be determined. The initial configuration of the production run of the simulation is taken as the reference configuration. Using this configuration, the least-square fittings of the successive trajectories are done to remove the rotational and translational motion in all the surfactant tails. Thus the entropy comes out to be the internal configurational entropy of the particles where the averaging is carried out over all surfactant molecules and all time frames of the production run.

Tilt vector and Voronoi diagram

The orientation of surfactant molecules in the bilayer and their location are understood by plotting tilt vector and Voronoi diagrams using MATLAB. Tilt vector is obtained by considering a vector joining the head and the end bead of a surfactant molecule present in the monolayer of the bilayer, which is projected on the bilayer surface. The projection of the vector onto two surfaces of the bilayer from each monolayer is represented as an arrow. The Voronoi cell areas are calculated using MATLAB and represent the area occupied by both BTMAC and SA head-groups. Tilt angles of BTMAC and SA chains are superimposed on the Voronoi cells to relate tilt with area per head group. The vector from tail to head, $\vec{r}_{th}$, is defined as,

$$\vec{r}_{th} = \vec{r}_h - \vec{r}_t \tag{4.7}$$

The tilt vector projected on the bilayer surface is defined as,

$$\vec{t} = \vec{r}_{th} - (\vec{r_{th}}.\hat{n})\hat{n} \tag{4.8}$$

Tilt angle, θ_{tilt}, is defined by,

$$< \theta_{tilt} >=< cos^{-1}\frac{\vec{r_{th}}.\hat{n}}{|\vec{r_{th}}|} > \tag{4.9}$$

where $\hat{n}$ is the unit vector and the angular brackets denote the time averaging. Similarly, the interdigitation, $I(x, y)$, in the surfactant chains is calculated by computing the difference in the z-co-ordinates of the end beads between the less and more populated leaflets as a function of the bilayer surface. Mathematically it is represented as,

$$I(x, y) = z_{L,end}(x, y) - z_{M,end}(x, y) \tag{4.10}$$

where $z_{L,end}(x, y)$ and $z_{M,end}(x, y)$ are the z coordinates of the end beads of less and more populated leaflets respectively.

Order Parameter

Since a united atom model is used for the current study, order parameter ($|S_{CD}|$) is calculated by the equation [Douliez *et al.*, 1998],

$$|S_{CD}| = \frac{2}{3}S_{xx} + \frac{1}{3}S_{yy} \tag{4.11}$$

$$|S_{xx}| \text{ or } |S_{yy}| = \frac{1}{2}(< 3cos^2\beta - 1 >) \tag{4.12}$$

Here β is the angle between the CD bond vector and the bilayer normal, $|S_{xx}|$ or $|S_{yy}|$ are the order parameters along the x or y directions respectively. Similarly, for coarse-grained beads, the order parameter is defined as P_2 and computed using the following equation,

$$P_2 = \frac{1}{2}(< 3cos^2\theta - 1 >) \tag{4.13}$$

Here θ represents the angle between the bond vector of two consecutive CG beads and the normal of the bilayer. The value of P_2 explains the alignment of beads with respect to the bilayer normal. If P_2 is 1, it shows a perfect alignment with direction of the bilayer normal, -0.5 means anti-alignment and 0 describes that the molecule is randomly oriented with respect to the normal of the bilayer.

4.4 RESULTS AND DISCUSSION

All initial configurations self-assemble to asymmetric bilayers. The atomistic simulations show that different initial configurations result into interdigitated asymmetric bilayers at 283 K. For all of the self-assembled bilayers, the percentage of asymmetry, λ, is calculated according to equation 4.1. The percentage of asymmetry in each of the AA and CG system is shown in table A1 in the appendix. For the bilayers prepared from biased configurations, the asymmetry ranges from 27.6% in S1 to 2.66% in S8 with an intermediate asymmetry of 12.06% in S5. The initial configuration of AA S5 is a symmetric bilayer, which transforms into an asymmetric rippled bilayer within initial few ns of the AA simulation due to the tilting and tumbling of few molecules within the interdigitated region by the thermal fluctuations. Since local instabilities are induced in the symmetric bilayer as its initial configuration, few chains tumble to generate the rippled phase and the symmetry disappears. Once, the bilayer is asymmetric, it remains asymmetric throughout the AA run. Small numbers of molecules tumble in the initial 200 ps of the 5.5μs CG simulation of S5 and the asymmetry percentage changes a little from 12.06 % to 12.5 % and then remains same till the end of the NPT runs. The extent of asymmetry remains conserved from AA to CG simulations for remaining systems as presented in table 4.1 since there is no flip-flop event after the equilibration period of the AA runs and during the CG runs.

Studies have shown that flip-flop is possible in protein-free model membranes but the flip-flop is even too slow across the fluid phase due to the unfavorable passage of lipid head groups across the hydrophobic region of a bilayer[Karin *et al.*, 2002; F.-Xabier *et al.*, 2010; Allhusen and Conboy, 2017]. Many experiments have been carefully conducted before the flip-flop so that asymmetry can be probed [Collins and Keller, 2008; Pautot *et al.*, 2003; Kiessling *et al.*, 2006; Garg *et al.*, 2007]. Following similar line, we do not aim to probe a flip-flop in our simulations, instead, analyze lateral organizations in the bilayers [Perlmutter and Sachs, 2011]. Figure 4.2 (a)-(h) show the CG snapshots of the lamellar phases in decreasing order of asymmetry for all the systems investigated.

Table 4.3: Extent of interdigitation ($O_{overlap}$) of simulated bilayers at AA and CG resolutions. S6 is prepared only for CG runs as the system size is large.

System	AA	CG
S1 (Maximum asymmetry, 2D ripple)	0.72	0.67
S2 (Maximum asymmetry, 1D ripple)	0.76	0.77
S3	0.77	0.75
S4	0.87	0.81
S5 (Intermediate asymmetry, 2D ripple)	0.46	0.42
S6 (Intermediate asymmetry, 2D ripple, larger size)	-	0.43
S7 (Minimum asymmetry)	0.80	0.81
S8 (Minimum asymmetry)	0.73	0.74

Bonded distributions

AA and CG bonded distributions match well.
To validate the bonded potentials in the derived CG model, distributions due to bonds and angles of BTMAC and SA are calculated from both AA and respective CG simulations for all the systems and shown in figure 4.3. The CG distributions of BTMAC bonds match well to the respective AA distributions. The first two bonds of BTMAC show either a double peak or a shoulder and

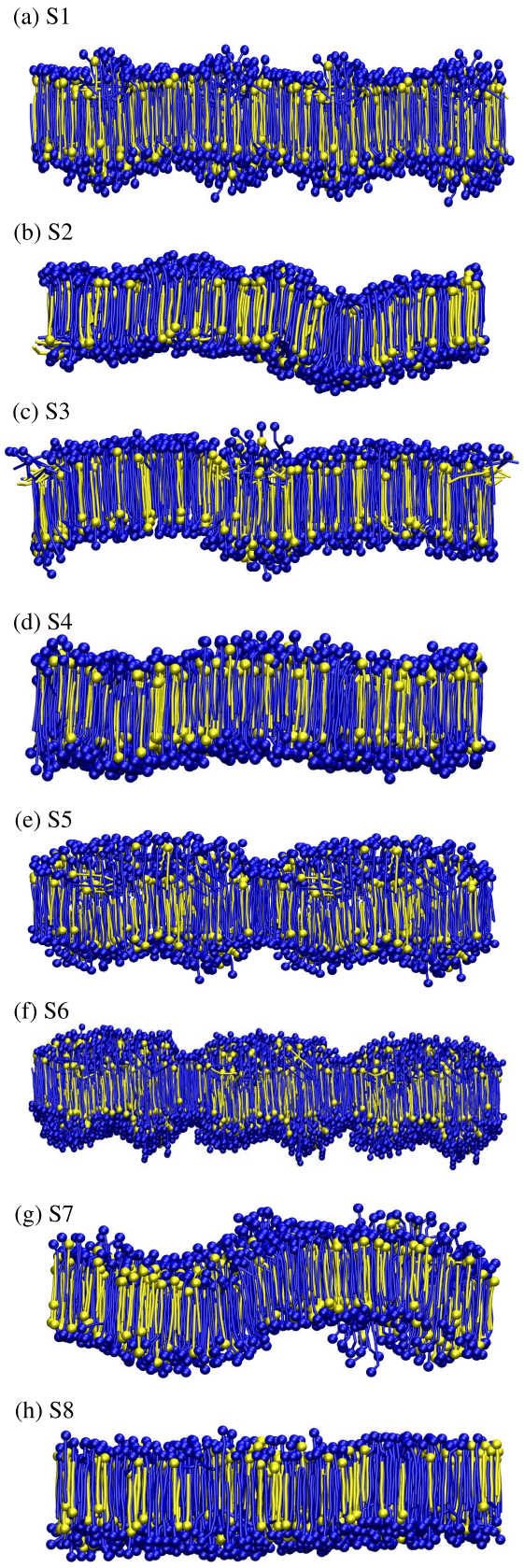

Figure 4.2: Final configurations of all asymmetric bilayers obtained from CG simulations. (a), (e), (f) and (g) correspond to bilayers S1, S5, S6 and S8 respectively obtained from biased configurations. Bilayers S2, S3, S4 and S7 obtained after self-assembly from random initial configurations are shown in (b), (c), (d) and (h) respectively. Similar configurations are observed from AA simulations.

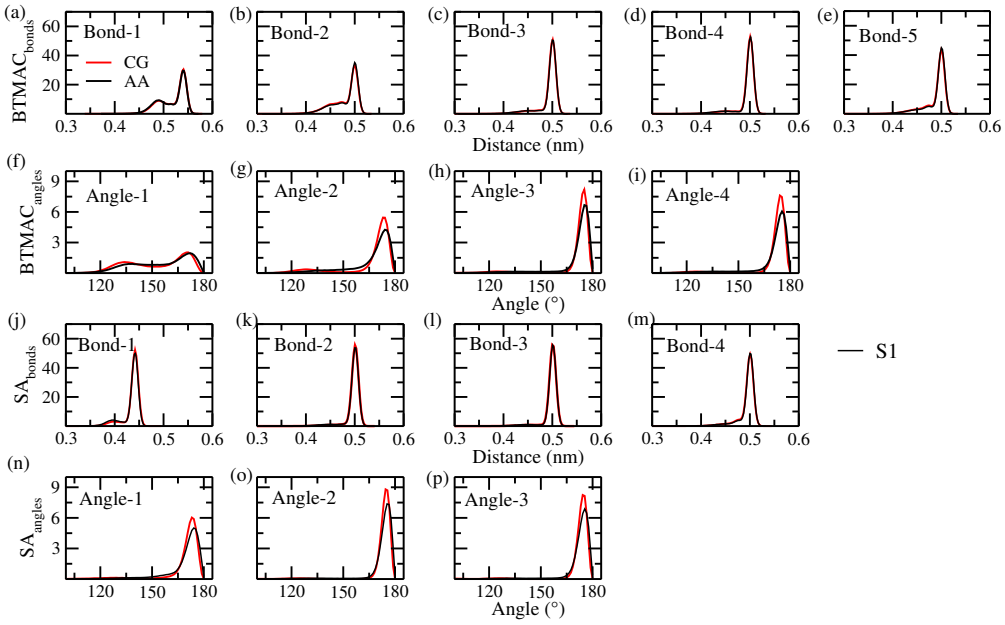

Figure 4.3: AA and CG bonded distributions of BTMAC and SA in maximum asymmetry bilayer S1. (a)-(e): BTMAC bonds, (f)-(i): BTMAC angles, (k)-(n): SA bonds and (o)-(q): SA angles. AA and CG bonded distributions are in good agreement with each other.

a peak suggesting two possible bond-lengths. This indicates existence of few BTMAC molecules having shorter bond-lengths compared to the remaining molecules. Similar behavior is observed for the first bond of SA. For rest of the bonds of both BTMAC and SA, single peak distributions are obtained in both resolutions. Similar to bonded distributions, the CG angle distributions match well to their respective atomistic distributions. The first BTMAC angle formed between initial two bonds of BTMAC have wider distributions. Remaining angles of both BTMAC and SA follow single peak distributions in both resolutions. Few BTMAC molecules can bend around second beads to make their chain lengths comparable to that of the SA generating wider distributions of the first angle. All other peaks of angle distributions are located near 180° demonstrating the stretched configurations. A good match in the AA and CG angle distributions of BTMAC and SA validates that the derived CG bonded potentials using the tabulated scheme works well under the assumptions taken in deriving the CG bonded potentials (equation 3.1). All bonded potentials are available online [Srivastava and Debnath, 2020].

Asymmetry and Density distributions

MARTINI force-field is suitable to reproduce the interdigitated CG lamellar phase. For a better understanding of the structure of the lamellar phases, a density profile of BTMAC and SA is calculated along the bilayer normal. Figures 4.4 (a) and (b) illustrate the density distributions of S1 and S2 bilayers with same maximum asymmetry generated from different initial configurations. Differences in the peak heights between two monolayers in figure 4.4 (a), (b) demonstrate the asymmetry at both scales. The less populated layer (shown in green color in figure 4.4 (a, b)) develops a hump and a peak suggesting the presence of more bent molecules in one layer than the other making the system asymmetric. The bent configurations of these molecules increase respective area per head group and create empty spaces in the hydrophobic region. This results in a drop in densities of chains along the bilayer normal. Since empty spaces in the hydrophobic region are not energetically favorable, molecules from the other leaflet fill the gap and keep the interdigitation and asymmetry intact. Similar interdigitation in single tail lipids

are obtained by dissipative particle dynamics when the interaction strength between head groups are tuned [Kranenburg *et al.*, 2003].

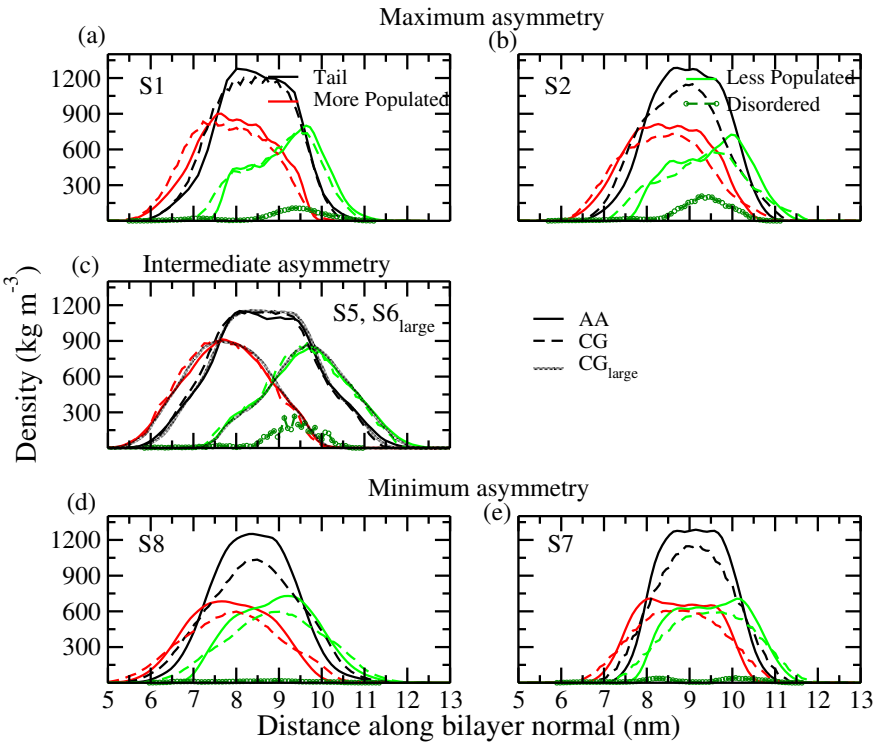

Figure 4.4: Density distributions of all BTMAC and SA along the bilayer normal in system with (a, b) maximum asymmetry, (c) intermediate asymmetry (d, e) minimum asymmetry. Solid lines: AA, dashed lines: CG. red and green: two monolayers including head to tail in a chain. Black: tails excluding the head groups. Dark green : CG molecules with high entropies.

Figure 4.4 (c) shows the density distributions of the bilayers with intermediate asymmetry where S6 has same compositions as S5, but larger in size. The system size does not affect the density profile. The height differences in densities of two leaflets is minimum for the minimum asymmetric bilayers (figures 4.4 (d) and (e)). Density profiles in figure 4.4 show strong overlaps between two monolayers. This demonstrates the presence of an interdigitated lamellar phase for each case. The extent of interdigitation, $O_{overlap}$, for all cases studied here is calculated using equation 4.2 (table 4.3). The variation in interdigitation from maximum to minimum asymmetric bilayer is moderate since interdigitation is averaged over all surfactant molecules along undulations discussed in the next section. The interdigitation is found to be approximately conserved across AA and CG simulations. To understand the location of chloride ions in the systems and to verify their equilibrations, density distributions of ions and BTMAC heads from both AA and CG simulations for both equilibration and production runs are shown in figures A1 and A2 respectively in the appendix. The locations of the ions do not change from equilibration to production runs as the negatively charged chloride ions prefer to stay closer to the positively charged BTMAC head-groups due to strong electrostatic interactions. The reasonable match in AA and CG density profiles validates that the CG bonded potentials derived from our AA simulations in combination with the non-bonded MARTINI force-field are suitable for capturing the atomistic interdigitated lamellar phase.

Bilayer properties

Formation of 1D/2D ripple phase at higher asymmetry percentage. The bilayer thickness calculated by equation 4.4 are superimposed on the Voronoi area per head group at both levels of resolutions (figure 4.5) for the bilayers prepared using biased configurations. Figures 4.5 (a), (b) and (d), (e) reveal the presence of two dimensional rippling in systems with maximum asymmetry (S1) and intermediate asymmetry (S5) whereas the bilayer with minimum asymmetry (S8) shows absence of rippling in both resolutions (figure 4.5 c)-f)). Although it is well known that

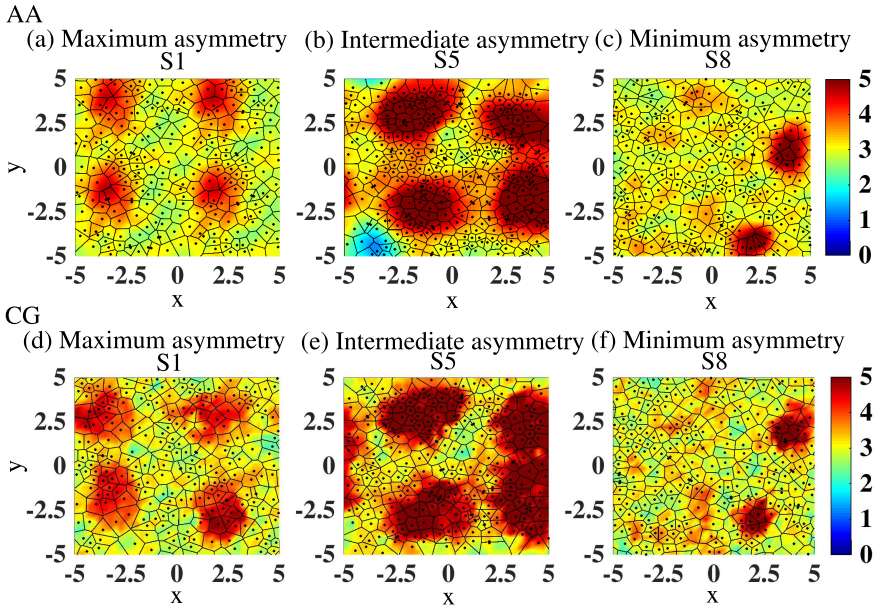

Figure 4.5: Bilayer thickness superimposed on the Voronoi area per head group in AA (a-c) and CG (d-f) resolutions for bilayers prepared from biased configurations. The unit of color-bar is in nm.

MARTINI model for lipid bilayers does not produce a ripple phase, re-parameterization of head to tail bead diameter may better capture phases of saturated lipids [Kranenburg and Smit, 2005; Rodgers *et al.*, 2012]. In our present study, the thickness varies between $3-5$ nm (color bar in figure 4.5) for S1 and S5 with clear two dimensional periodic behavior in both AA and CG resolutions. Similar variation in thickness has been observed earlier for a 2D rippled bilayer consisting a different ratio of BTMAC to SA molecules [Debnath *et al.*, 2014]. Previous AA simulations and experiments suggest similar thicknesses ~ 4.49 nm and ~ 4.1 nm respectively for the major arm (the region with no interdigitation) of a rippled DMPC bilayer [Khakbaz and Klauda, 2018; Akabori and Nagle, 2015]. Thus our CG model using non-bonded MARTINI force-field works well in reproducing a ripple-like phase as in the AA simulation. However, the thickness fluctuations are minimum for the minimum asymmetric bilayer for both AA and CG simulations (figures 4.5 (c) and (f)).

A similar behavior is seen for the interdigitation superimposed on the Voronoi area per head groups in figures 4.6. Interdigitation is calculated using equation 4.10. Therefore, zero to positive values indicate non overlapping region and negative values are identified as interdigitation. Similar method has been followed to identify rippling for a DMPC bilayer [Khakbaz and Klauda, 2018]. The bilayers S1 and S5 show a variations in interdigitation along 2D from ∼-1.8-0.6 nm confirming 2D ripple whereas system S8, with minimum asymmetry, does not show such a periodic behavior. The variations in interdigitations of S1 and S5 signify that these bilayers are made up of both highly packed regions (blue color) and has also free spaces where the chains do not interdigitate (red color) and hence form a 2D ripple phase or a square phase at both AA and CG levels. The regions of high interdigitation lead to strong packing of surfactant chains in bilayers with decrease

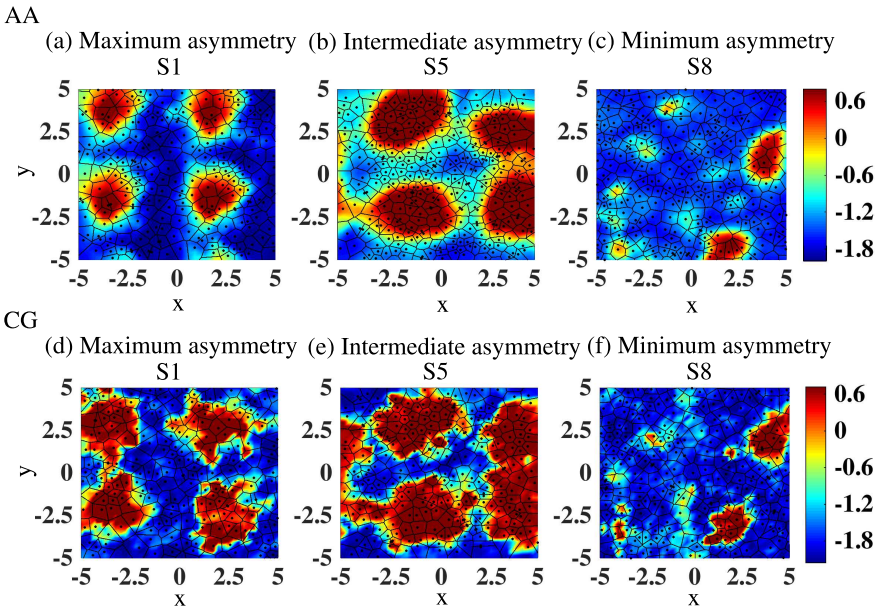

Figure 4.6: Interdigitation superimposed on the Voronoi area per head group in AA (a-c) and CG (d-f) resolutions for bilayers prepared from biased configurations. The unit of color-bar is in nm.

in bilayer thickness. Next to these regions, there are micro-domains with less interdigitation and larger thickness where chains have free spaces within two leaflets. This results in 2D periodic variations of larger hydrophobic barrier and interdigitated regions restricting chains to flip-flop and thus asymmetry is maintained. The behaviors of interdigitation and bilayer thickness are examined for a larger CG bilayer, S6 (table 4.1) which has same compositions as S5. The larger bilayer S6 also shows 2D rippling. Thickness of the maximum and minimum asymmetric bilayers

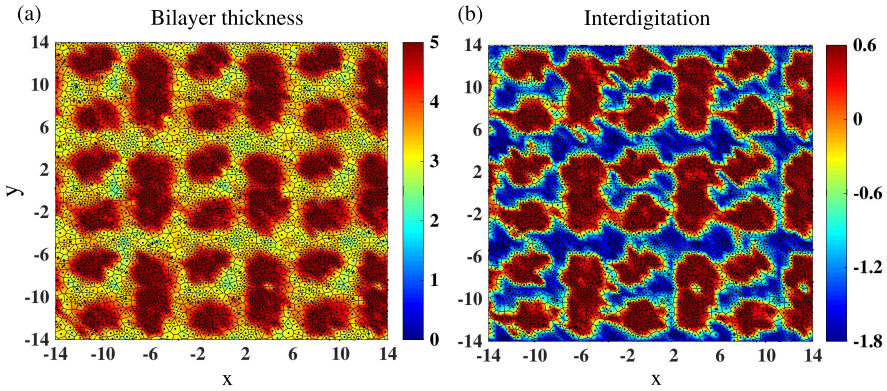

Figure 4.7: Thickness (a) and interdigitation (b) superimposed on the Voronoi cells in CG resolution for larger bilayer (S6) with intermediate asymmetry. The unit of color-bar is in nm.

obtained from random initial configurations are superimposed on the Voronoi area per head group for both AA and CG simulations. The thickness slightly varies between $3-4$ nm (color bar in figure 4.8) for the maximum asymmetric bilayer with a periodic variation along one direction. No periodic variation is observed for minimum asymmetric bilayer. A similar behavior is seen for the interdigitation shown on the Voronoi area per head groups (figure 4.9) where S2 shows a slight periodic patch along x-direction while S7 has no clear periodic patch at both AA and CG scales. A comparison between figure 4.8 and figure 4.9 again shows that the regions having higher interdigitation are more tightly held causing a reduction in bilayer thickness. The time averaged

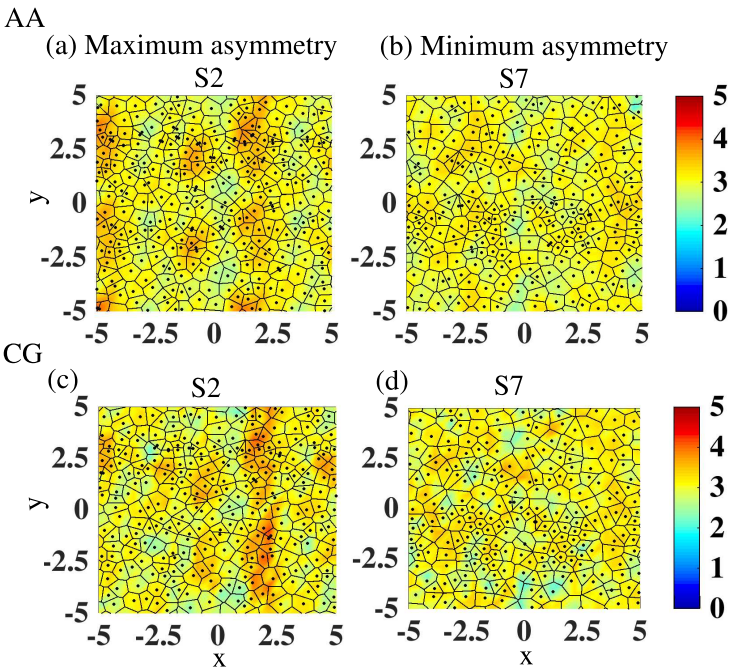

Figure 4.8: Bilayer thickness superimposed on the Voronoi area per head group for bilayers resulting from random initial configurations with maximum and minimum asymmetries. (a), (b): AA; (c), (d): CG. The unit of color-bar is in nm.

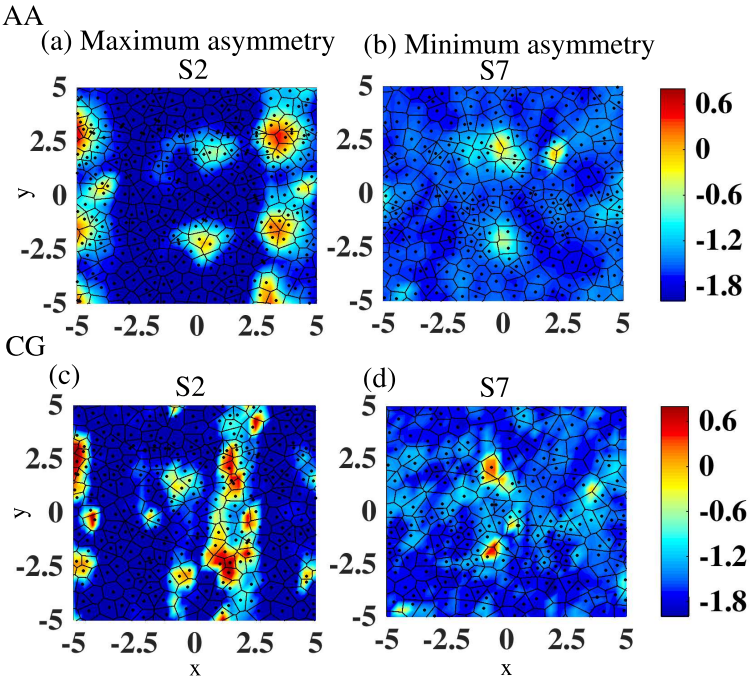

Figure 4.9: Interdigitation superimposed on the Voronoi area head per group for bilayers resulting from random initial configurations with maximum and minimum asymmetries. (a), (b): AA; (c), (d): CG. The unit of color-bar is in nm.

bilayer thickness and interdigitations for all the bilayer investigated here are presented in table 4.4 and table 4.3 respectively. Note, that S1 and S2 have same extent of maximum asymmetry

Table 4.4: Bilayer thickness (in nm) from AA and CG simulations.[a][Lunkad *et al.*, 2017], [b][Ritwiset *et al.*, 2016], [c][Khakbaz and Klauda, 2018], [d][Zhao *et al.*, 2019], [e][Takahashi *et al.*, 1997].

System	AA	CG
S1 (Maximum asymmetry)	3.21 ± 0.48	3.33 ± 0.53
S2 (Maximum asymmetry)	3.10 ± 0.31	3.08 ± 0.34
S3	3.08 ± 0.33	3.12 ± 0.38
S4	2.82 ± 0.22	2.99 ± 0.32
S5 (Intermediate asymmetry)	3.85 ± 0.92	3.96 ± 0.89
S6 (Intermediate asymmetry)	-	3.94 ± 0.90
S7 (Minimum asymmetry)	3.01 ± 0.19	2.99 ± 0.30
S8 (Minimum asymmetry)	3.18 ± 0.47	3.15 ± 0.54
Simulation results from literature	Surfactant-cosurfactant, BTMAC-SA, gel 3.14±0.09[a] Non ionic surfactant, Span-60, gel 3.00±0.004[b] Lipid, DMPC, ripple 4.49±0.02[c] Cationic surfactant, DIDMAMS-CMR, ripple 3.352[d]	
Experiment results from literature	Lipid, DHPC gel 2.98[e] Lipid, DMPC ripple ∼4.19[c]	

but form 2D and 1D rippled phases as seen from figures 4.5(a),(d) and 4.8(a),(d) respectively. This indicates that the differences in initial configurations of the systems lead to the topological differences in the final configurations. Similar to this, two different initial conditions, one as a biased bilayer and another is random lipid insertion, lead to different final configurations of the aggregates of lipids, although no rippling is observed there [Xue *et al.*, 2018].

Rippled phase is stable while heating close to physiological temperature The effect of temperature is investigated for AA bilayers S1 (maximum asymmetry), S5 (intermediate asymmetry) and S8 (minimum asymmetry). The interdigitations superimposed on Voronoi area per head group for these three bilayers are shown in figure 4.10. S1 bilayer preserves two dimensional rippling as well as interdigitation and asymmetry after heating to 308 K and cooling back to 283 K (figure 4.10 a), d), g)). Unlike S1, while heating, the interdigitated domains of S5 across two leaflets shifts on the bilayer xy surface where the non-interdigitated regions become interdigitated and vice-versa. Although the interdigitated regions are shifted, two dimensional rippling is still present for S5 at 308 K which is well-conserved when cooled to 283 K for S5. Extent of interdigitation, $O_{overlap}$, marginally changes from 0.46 (table 4.3 to 0.50 once heated to 308 K and reduces to 0.472 when cooled back to 283 K. Although interdigitation in S5 is well maintained, asymmetry percentage changes from 12.06 to 13.26 while heating to 308 K and then to 14.05 at 283 K. This is because chains residing near the midplane tumble and traverse from one leaflet to the other while heating. This demonstrates that ripple phases generated from biased configurations in our simulations with variations in asymmetry are stable for a range of temperatures. The minimum asymmetric bilayer S8 preserves interdigitation and asymmetry percentage during the temperature change.

Configurational entropy per chain

Two distinct classes of molecules with higher and lower entropy per chain are present in the bilayers. Per chain configurational entropy, $S_{conf}^{per-chain}$, of BTMAC and SA tails

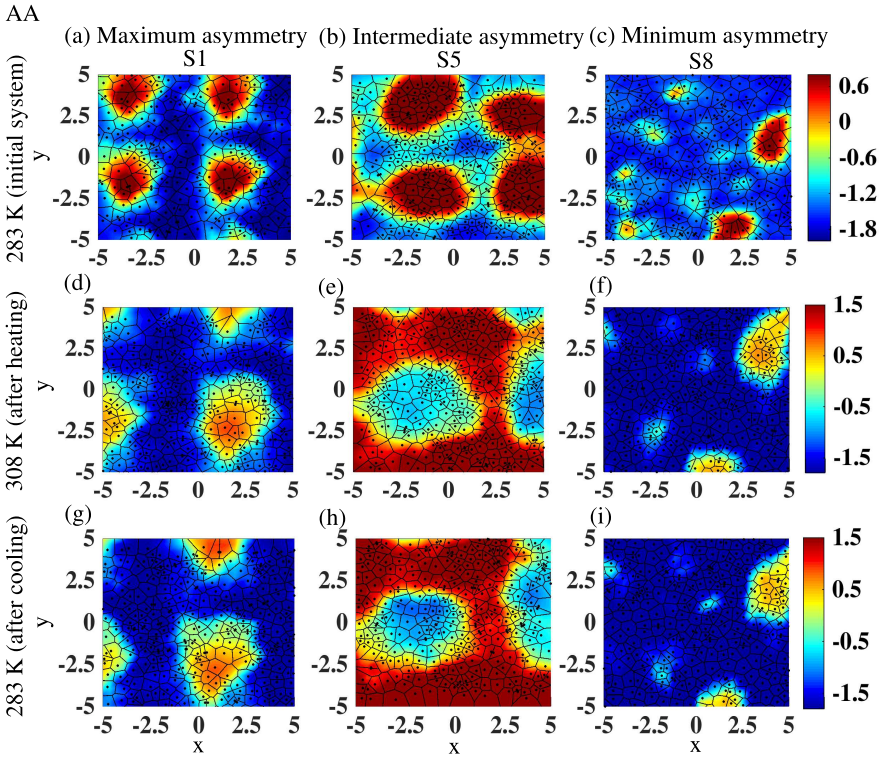

Figure 4.10: Interdigitation superimposed on the Voronoi cells at AA level for bilayers with maximum asymmetry (S1), intermediate asymmetry (S5) and minimum asymmetry (S8) at 283 K (a-c), after heating to 308 K (d-f) and after cooling back to 283 K (g-i). The unit of color-bar is in nm.

are calculated using equation 4.5 and shown in figures 4.11, figures 4.12 and 4.13 respectively. for maximum, intermediate and minimum asymmetric bilayers respectively. The entropies are found to be well converged within the analyzed run lengths for both AA and CG simulations. Two distinct values of entropies are obtained for all systems in AA level. Molecules having lower and higher $S_{conf}^{per-chain}$ are referred to as ordered and disordered BTMAC and SA molecules (table 4.5). Note, that the true entropy is overestimated using the quasi-harmonic approximation using equation 4.5 by neglecting anharmonicities and correlated motions. Due to the intermolecular correlations present in the systems, the entropy calculated is not the summation of the individual entropies of the surfactant molecules. However, these limitations are of lesser significance to our calculations since the differences in per chain entropies are more important to identify two classes of molecules, i.e. ordered and disordered molecules. Hence, these effects are expected to be cancelled out. The CG entropies are much lower than the respective AA entropies due to the lower degrees of freedom in the CG representations. The differences in entropies between the two classes of molecules reduce from AA to CG simulations. The values of $S_{conf}^{per-chain}$ of SA chains from our simulations are compared with the ones of DPPC acyl chains reported earlier since they have similar number of beads present in both AA and CG scales. $S_{conf}^{per-chain}$ of DPPC acyl chains in fluid phase ranges from $821 - 823$ J K^{-1} mol^{-1} and 178 J K^{-1} mol^{-1} at AA and CG scales respectively [Baron *et al.*, 2006]. $S_{conf}^{per-chain}$ of SA chains averaged over all ordered and disordered molecules from our calculations ranges from $431 - 500$ J K^{-1} mol^{-1} and $146 - 156$ J K^{-1} mol^{-1} at AA and CG scales respectively. These values are lower compared to DPPC lipids since the bilayers in our study are in interdigitated gel or rippled phase unlike the reported fluid phase of DPPC [Baron *et al.*, 2006]. Density profiles of these disordered molecules are calculated from CG simulations and are shown in figure 4.4. The disordered molecules are confined to the less populated layer of the maximum asymmetric bilayers S1 and S2. Since the disordered molecules do not traverse to the other leaflet as explained earlier,

Table 4.5: Average single chain configurational entropy, $S_{conf}^{per-chain}$, (JK^1mol^{-1}) with standard deviations calculated from time-frames over which $S_{conf}^{per-chain}$ converges and all molecules of BTMAC and SA in AA and CG simulations. All the values are rounded off to their nearest integers and the standard deviations smaller than 0.1 are not reported here.

Model	System	BTMAC ordered molecules	BTMAC disordered molecules	SA ordered molecules	SA disordered molecules
AA	S1 (Maximum Asymmetry)	697 ± 0.1	1100 ± 4	444 ± 0.2	738 ± 4
	S2 (Maximum Asymmetry)	667 ± 3	1095 ± 3	428 ± 2	864 ± 2
	S3	674 ± 1	1118 ± 2	435 ± 0.2	859 ± 1
	S4	688 ± 1	935 ± 16	435 ± 0.2	537 ± 6
	S5 (Intermediate asymmetry)	755 ± 1	1056 ± 2	453 ± 1	663 ± 5
	S7 (Minimum Asymmetry)	666 ± 1	933 ± 5	423 ± 0.4	611 ± 2
	S8 (Minimum Asymmetry)	695 ± 1	1015 ± 3	442 ± 0.6	795 ± 3
CG	S1 (Maximum Asymmetry)	230	285 ± 0.6	153	198 ± 0.2
	S2 (Maximum Asymmetry)	232	290 ± 0.9	155	189 ± 0.5
	S3	222	292 ± 0.6	149	198 ± 0.3
	S4	218 ± 0.1	286 ± 0.3	146	163 ± 0.1
	S5 (Intermediate asymmetry)	226 ± 0.1	274 ± 2	150	174 ± 0.3
	S6 (Intermediate asymmetry)	229 ± 0.1	304 ± 0.7	153	190 ± 0.9
	S7 (Minimum Asymmetry)	223 ± 0.1	284 ± 0.4	148	190 ± 1
	S8 (Minimum asymmetry)	226 ± 0.1	279 ± 0.2	147	196 ± 1

the maximum asymmetry is conserved. For the intermediate asymmetry bilayers, the population of the disordered molecules are less inhomogeneous across two layers compared to the case of the maximum asymmetry. The inhomogeneity in population of the disordered molecules disappears for the bilayer with the minimum asymmetry.

Tilt

Disorered molecules stay tilted in the less populated layer and their distributions become more homogeneous with lowering in asymmetry. To understand the tilt of both BTMAC and SA molecules in the two monolayers of a bilayer, the tilt vector is calculated using equation 4.8. The projections of the head to tail vectors on the two monolayer surfaces of final configurations of the bilayers are plotted considering both ordered and disordered molecules, identified based on $S_{conf}^{per-chain}$ as discussed above. Figures 4.14 and 4.15 show the tilt vectors for S1, S5 and S8 bilayers with biased initial configurations and for S2 and S8 with random initial

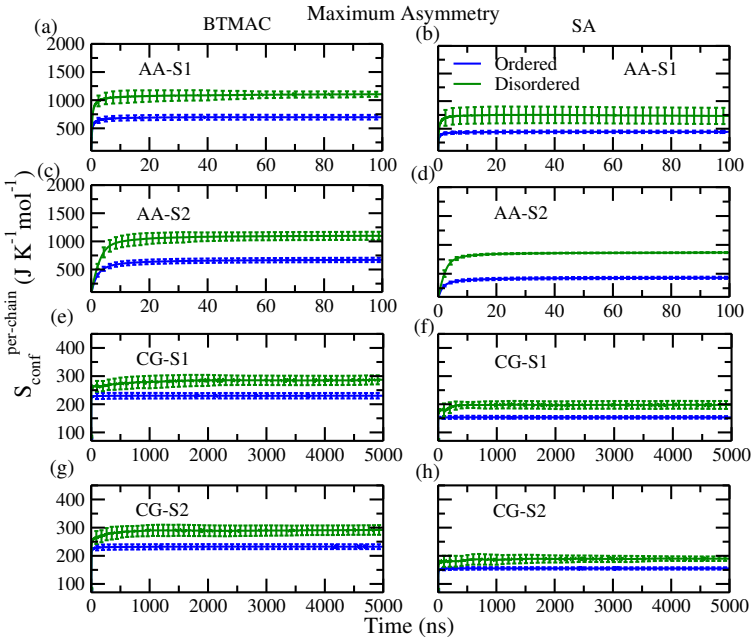

Figure 4.11: Time evolution of per chain configurational entropy of S1 and S2 with maximum asymmetry averaged over all molecules, (a)-(d) AA, (e)-(h) CG. Molecules with higher and lower entropies are referred to as disordered and ordered molecules. The error bars represent the standard deviations in per chain configurational entropies obtained from averaging over all the molecules.

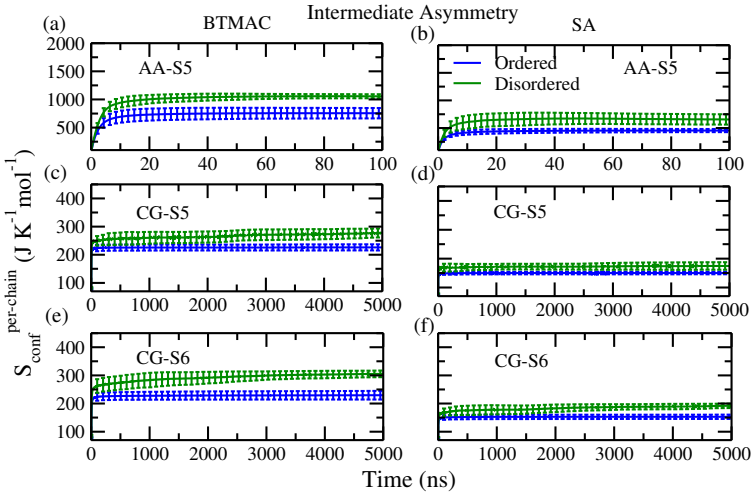

Figure 4.12: Time evolution of per chain configurational entropy of S5 and S6 with intermediate asymmetry, (a)-(d) AA, (e)-(h) CG. The error bars represent the standard deviation in per chain configurational entropy arising from averaging over all molecules in two classes.

configurations respectively. The ordered molecules in both the layers stay parallel to the bilayer normal throughout the simulation and hence the lengths of the respective head-to-tail arrows are smaller than that for the disordered molecules. For all the bilayers shown in figures S5 and S6, the less populated layer is found to have more disordered molecules with higher tilt (represented

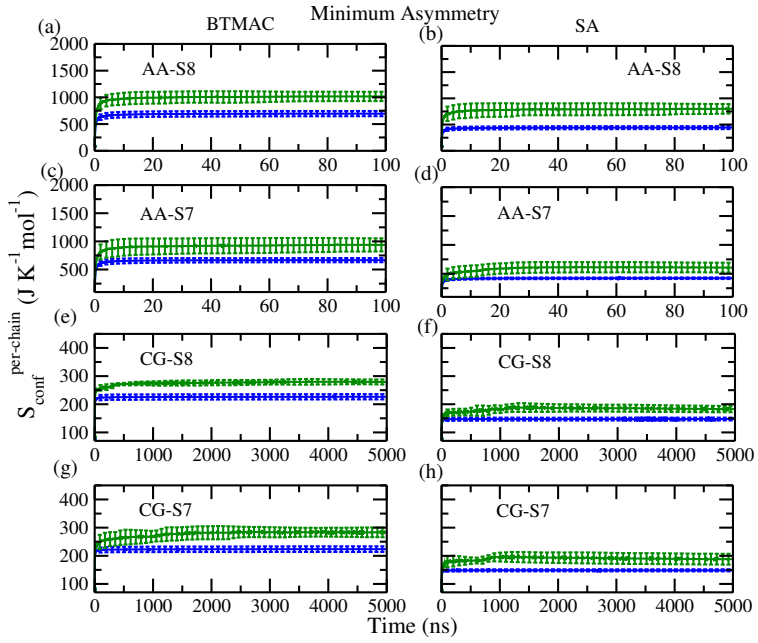

Figure 4.13: Time evolution of per chain configurational entropy of S8 and S7 with minimum asymmetry, (a)-(d) AA, (e)-(h) CG. The error bars represent the standard deviation in per chain configurational entropy arising from averaging over all molecules in two classes.

in green color). This is consistent with their respective density profiles (dark green lines in figure 4.4). As mentioned before, the monolayer of the maximum asymmetric bilayers (S1 and S2) with lower density is found to be more populated by the disordered molecules which are more tilted in both AA and CG resolutions. Figures 4.14 and 4.15 show that the disordered molecules (indicated by longer arrows) are more tilted and are present more in one layer compared to the other. The direction of the arrows indicates the rippling [Debnath *et al.*, 2014]. Tilting causes area expansion in one layer. To compensate that, total number of molecules in that specific layer decreases leading to asymmetry. Earlier electron density map of phospholipid bilayer has shown that differences in thickness in major and minor arms characterizes the asymmetric rippled bilayer (defined with respect to the bilayer normal) due to the mean chain tilt along the ripple wave vector [Sengupta *et al.*, 2001]. On moving from maximum to intermediate asymmetry bilayer (4.14), the disparity in population of disordered molecules across the two layers does not disappear, but reduces. Higher occupancy of disordered molecules in the less populated monolayer is again found in intermediate asymmetric bilayers at both AA and CG levels. Chains in the minimum asymmetric bilayer are less tilted compared to the ones in the intermediate asymmetric rippled bilayer. Both the leaflets of the minimum asymmetric bilayers are almost uniformly occupied with less number of disordered molecules. This is in agreement with the density profile of disordered molecules shown in figure 4.4 (d) and (e). From figures 4.14 and 4.15, it is noted that the population difference of the disordered molecules across two layers reduces as asymmetry reduces at both AA and CG levels.

Next, the time averaged tilt vectors of the more populated leaflets are computed at the CG levels for 1D ripple in S1 (maximum asymmetry), 2D ripple in S5 (intermediate asymmetry) and gel phase in S8 (minimum asymmetry) and are superimposed on respective bilayer thicknesses (figure 4.16). For 1D ripple, the tilt vectors follow curvilinear paths with a predominant orientation along x, the direction of rippling. The arrow heads for the 2D rippled bilayer show a swirling pattern encompassing both x and y directions. The tilt vectors are strictly oriented along one direction without any swirling for the gel phase. Thus, a systematic variation in collective directions of the time averaged tilt vectors clearly distinguishes between 1D, 2D rippled and gel phases.

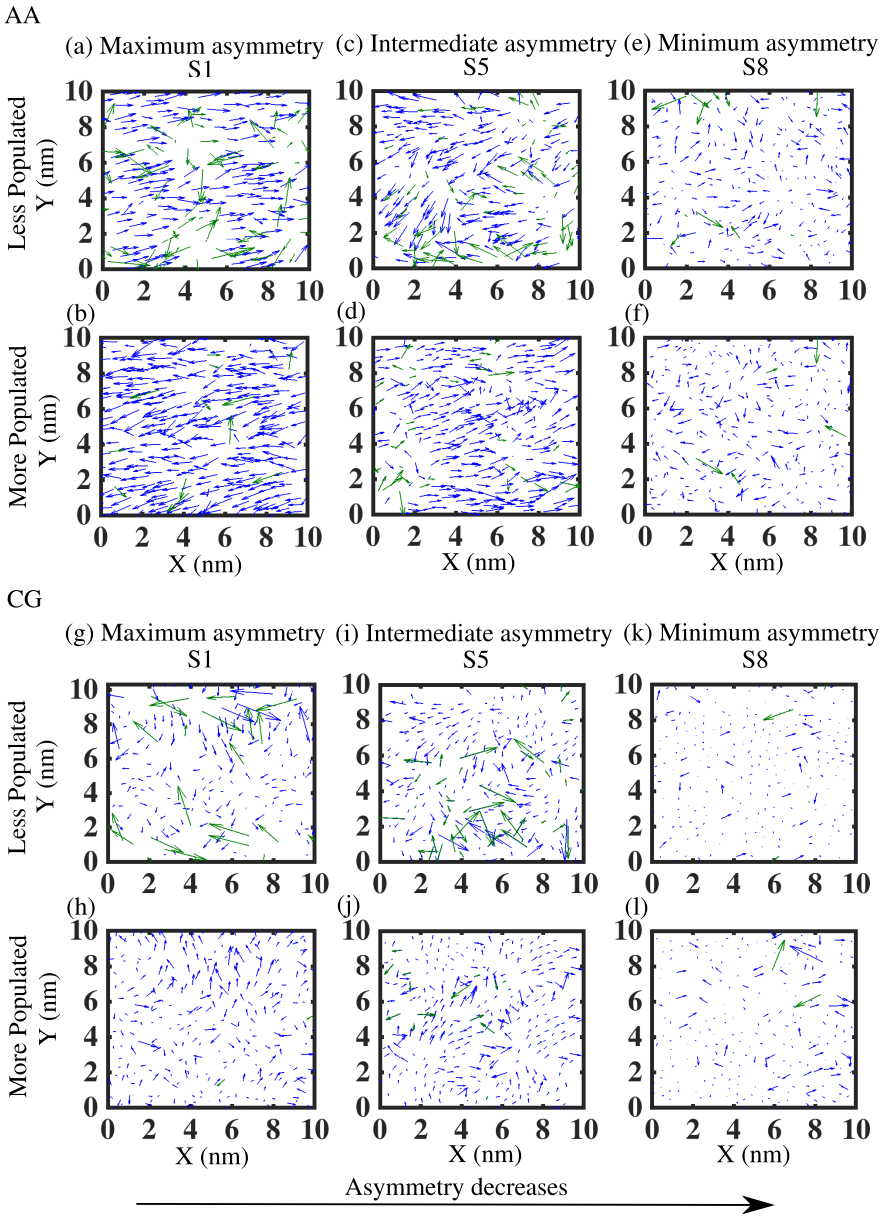

Figure 4.14: Tilt vectors ($\vec{t}$) of BTMAC and SA for less and more populated leaflets for the final configurations of bilayers created using Packmol. Blue arrows: ordered molecules, green arrows: disordered molecules. (a), (b): maximum asymmetry, (c), (d): intermediate asymmetry and (e), (f) minimum asymmetry at AA resolution. Similarly tilt vector in the CG resolution is shown in (g), (h): maximum asymmetry, (i), (j): intermediate asymmetry and (k), (l).

Order parameter

Difference in order parameter across leaflets induces asymmetry The order parameter, $|S_{CD}|$, calculated using equation 4.11 for all the AA asymmetric bilayers in this study is reported in table 4.6. Similar values of AA $|S_{CD}|$ is found for the gel phase of a bilayer comprised of BTMAC and SA obtained from previous simulations [Lunkad *et al.*, 2017; Debnath *et al.*, 2009] and the gel phase is verified by differential scanning calorimetry experiments [Debnath *et al.*, 2009]. The order parameter of a liquid gel phase of a DMPC bilayer containing 40% cholesterol is found to lie within $\sim 0.3 - 0.45$ and that of a solid gel phase of PE bilayers lie within $\sim 0.2 - 0.42$ [Boughter

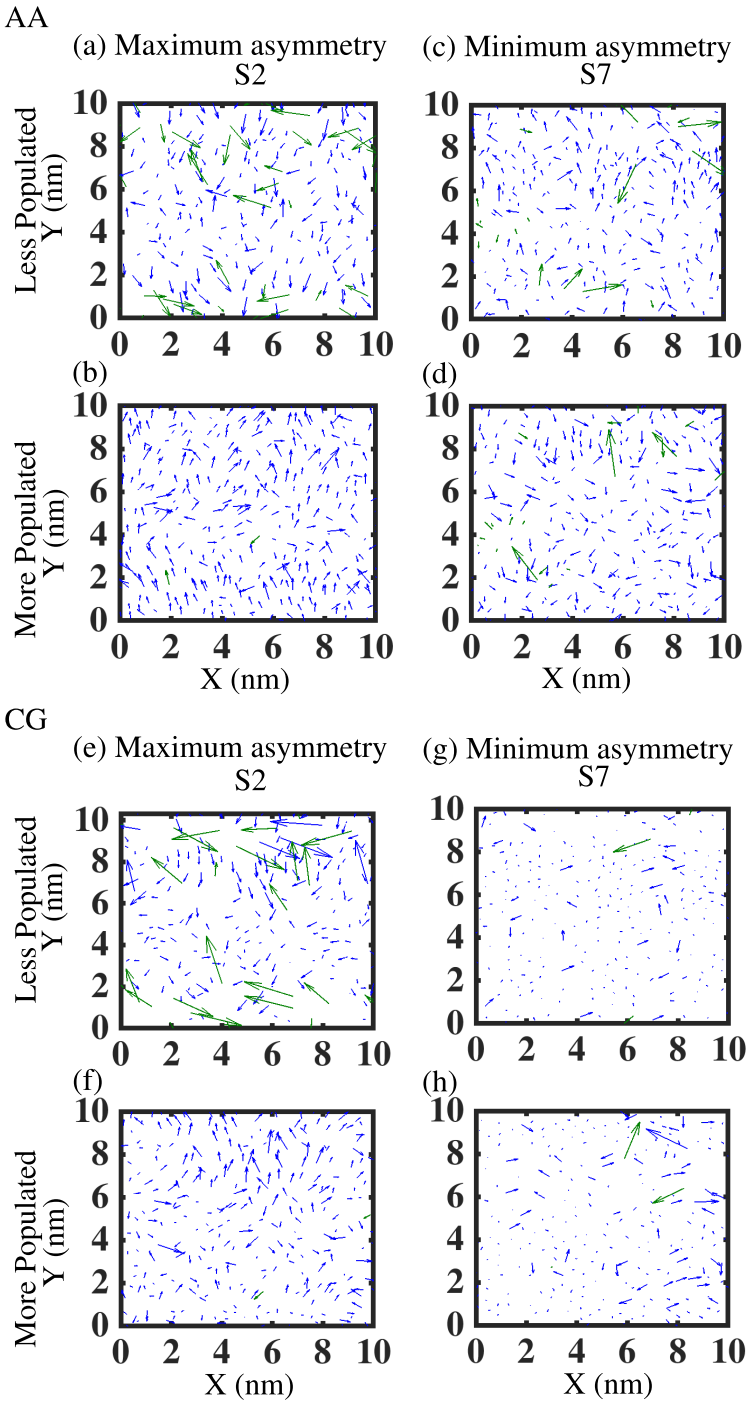

Figure 4.15: Tilt vectors ($\vec{t}$) of BTMAC and SA for less and more populated leaflets for the final configurations of bilayers with random initial configuration. Bilayer S2 has maximum asymmetry whereas S7 has minimum asymmetry. Blue arrows: ordered molecules, green arrows: disordered molecules. (a), (b): maximum asymmetry, (c), (d): minimum asymmetry at AA resolution. (e), (f): maximum asymmetry; (g), (h): minimum asymmetry at CG resolution.

et al., 2016]. Similarity in $|S_{CD}|$ between bilayers in our study and DMPC bilayers at gel phase reported earlier indirectly confirms that our AA bilayers are in gel phase. The order parameter of a rippled DMPC bilayer is found to be $\sim 0.1 - 0.39$ [Khakbaz and Klauda, 2018]. Therefore, the difference between a gel and ripple phase is not clear from the $|S_{CD}|$ values obtained from our

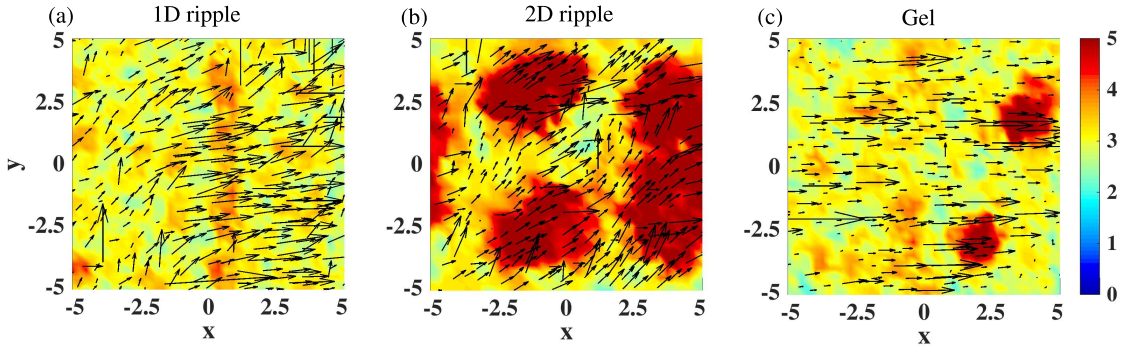

Figure 4.16: Time averaged tilt vectors ($< \vec{t} >$) of BTMAC and SA for more populated leaflets for the bilayers with (a) Maximum asymmetry, 1D ripple (system S2), (b) Intermediate asymmetry, 2D ripple (system S5) and (c) Minimum asymmetry, Gel phase (system S8). The tilt vectors are superimposed on the bilayer thicknesses. The unit of colorbar is in nm.

studies. Rippling is identified based on the periodic behavior in the thickness and interdigitations as discussed before. The rippled bilayer has an alternate gel-like strongly interdigitated and disordered non-interdigitated regions.

Next, P_2 is calculated using equation 4.13 for both BTMAC and SA at both the scales. Values of P_2 match well with the ones reported earlier in table 4.7. The effect of compositional asymmetry on the order parameter across two leaflets of a bilayer is investigated by calculating the order parameter, P_2, separately for more and less populated layers. Figures 4.20 shows the P_2 averaged over all BTMAC and SA present in each leaflet of all the bilayers. In both resolutions, the difference in P_2 across two leaflets of a bilayer can be clearly visible from figure 4.20. Bilayers S1 and S2 exhibit the highest asymmetry and due to the population differences across two leaflets, the APS (area per surfactant) is higher in one leaflet (shown in table 4.2). The penalty due to differences in APS across the leaflets is released via curvature formation in the bilayers resulting in ripple phases. Very high asymmetry results in non-uniform tilt across two leaflets, shown in figures 4.17 and 4.18. This leads to a weak packing in the chains resulting in high difference in P_2 and moderate interdigitation (table 4.3). A significant difference in P_2 across two leaflets (ΔP_2) has been observed for S1 to S6 bilayers. Interestingly S4 has similar order in both leaflets at AA and CG levels as there is no noticable change in bilayer tilt for S4 across two layers (figure 4.19). A decreasing asymmetry in S4 compared to S1-S3 leads to less population difference. S4 does not exhibit non-zero ΔP_2 as compositional asymmetry in S4 influences a complementary area per head group expansion across two leaflets with higher extent of interdigitation instead of a difference in tilt or in order parameter (figure 4.19). Thus, the increased APS of S4 (table 4.2) results in the minimum bilayer thickness (table 4.4) causing strong chain packing and interdigitation (table 4.3). The strong packing avoids curvature and hence the bilayer is in asymmetric interdigitated gel phase. As S5 and S6 have least APS, their bilayer thickness are highest (tables 4.2 and 4.4) leading to poor packing and minimum interdigitations. The similarity in the order parameters due to tilt symmetry across two leaflets of the minimum asymmetric bilayers (S7 and S8) indicates that the two layers of the bilayer to be phase symmetric. Although individual leaflets may have tilt variations (figures 4.17 and 4.18) in S7 and S8 leading to less interdigitation in S7 and S8 than in S4, the average tilt remain similar across two leaflets. Compositional asymmetry induces difference in order parameter across two leaflets in both AA and CG mixed surfactant bilayers. Hence the phase asymmetry across the two leaflets decreases as the compositional asymmetry decreases except S4.

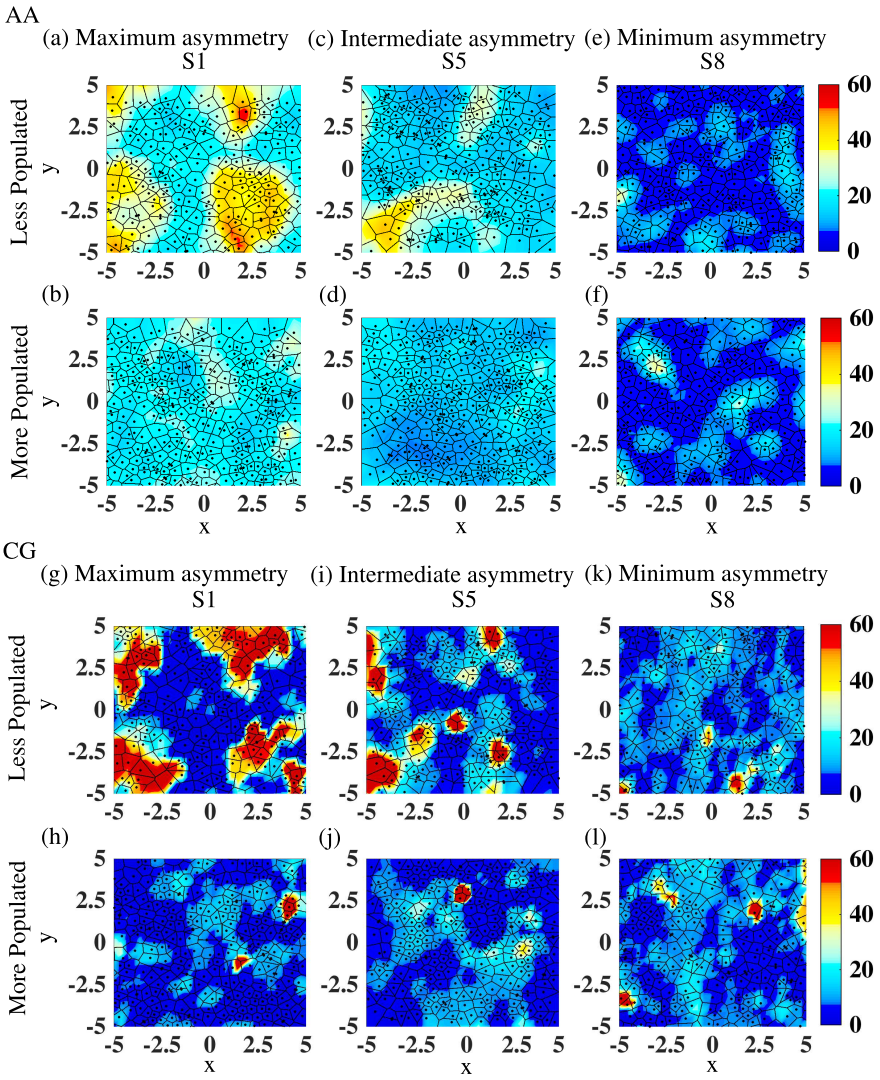

Figure 4.17: Time averaged tilt angles superimposed on the Voronoi cells of less and more populated leaflets in AA resolution for the bilayers with lamellar phase as the configuration (a), (b): maximum asymmetry; (c), (d): intermediate asymmetry and (e), (f) minimum asymmetry in AA resolution. Similarly (g), (h): maximum asymmetry; (i), (j): intermediate asymmetry and (k), (l) minimum asymmetry in CG resolution. The unit of colorbar is in degree(°).

Entropy and bilayer properties

Asymmetry is driven by entropy which is reflected in bilayer properties such as, interdigitation, thickness and order parameter. The influence of $S_{conf}^{per-chain}$ on the physical properties of the bilayers are investigated further. $S_{conf}^{per-chain}$ is calculated for the surfactant tails because tails undergo higher extent of rearrangements in order to maintain the structure and stability of the bilayer through hydrophobic attractions. $S_{conf}^{per-chain}$ averaged over all ordered and disordered tails and over last 50 ns/5μs time for AA/CG simulations are plotted with respect to asymmetry percentage in figure 4.21. The magnitudes of the error bars are smaller in the CG resolution than that in the AA resolution for both BTMAC and SA, due to the less degrees of freedom in CG systems. The configurational entropies of the tails increase with asymmetries in the bilayers in both AA and CG resolutions indicating that the asymmetry in the bilayers is generally entropically favorable.

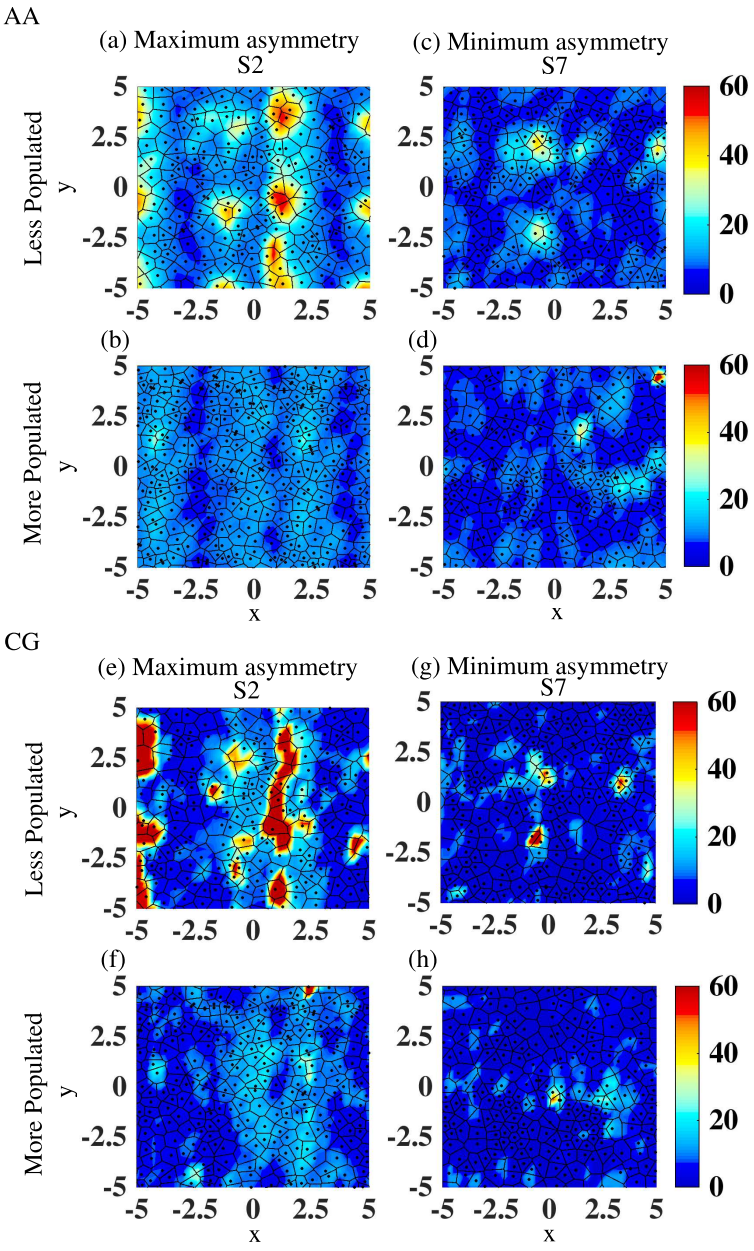

Figure 4.18: Time averaged tilt angles superimposed on the Voronoi cells of less and more populated leaflets for the bilayers with random initial configurations. (a)-(d) AA, (e)-(h) CG. The unit of colorbar is in degree(°).

$S_{conf}^{per-chain}$ are plotted with respect to the interdigitation and bilayer thickness (figure 4.22) at both AA and CG resolutions. As bilayer interdigitation increases, chains are tightly bound and packed, resulting in lowering in $S_{conf}^{per-chain}$ with increasing order. An increase in interdigitation is reflected in decrease in bilayer thickness. Since the interdigitation in the bilayer linearly decreases (and thickness linearly increases) with $S_{conf}^{per-chain}$, change in $S_{conf}^{per-chain}$ can be measured from the physical properties of the bilayers (figures 4.22). As $S_{conf}^{per-chain}$ lowers with increase in order, $S_{conf}^{per-chain}$ is plotted with respect to (1-P_2^2) in figure 4.23 and found to follow an empirical relation as follows,

$$S_{conf}^{per-chain} = S_0 + B_0 R(1 - P_2^2) \tag{4.14}$$

Here, S_0 is the available entropy of the chains when they are perfectly ordered (P_2=1) and is analogous to the residual entropy in protein systems [Li *et al.*, 1996; Trbovic *et al.*, 2009].

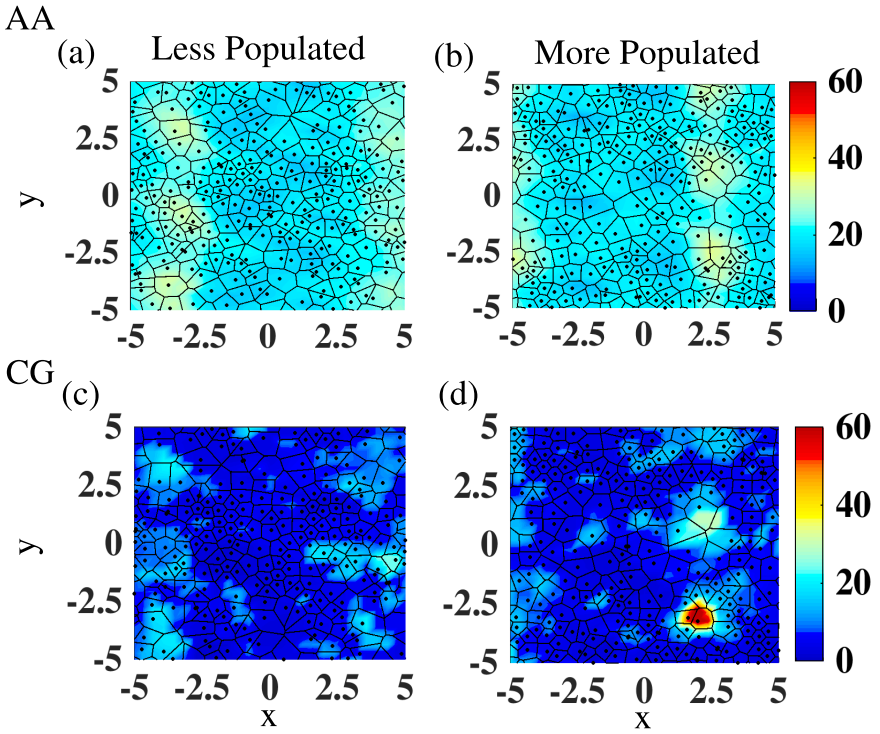

Figure 4.19: Time averaged tilt angles superimposed on the Voronoi cells of (a)-(b) AA and (c)-(d) CG bilayer S4. The unit of colorbar is in degree(°).

Table 4.6: Average order parameter, $|S_{CD}|$ of simulated bilayers at AA resolutions. [a][Debnath *et al.*, 2009], [b][Lunkad *et al.*, 2017], [c][Khakbaz and Klauda, 2018], [d][Zhao *et al.*, 2019], [e][Davis, 1979]

System	BTMAC	SA
S1 (Maximum asymmetry)	0.32 ± 0.03	0.36 ± 0.01
S2 (Maximum asymmetry)	0.41 ± 0.05	0.43 ± 0.01
S3	0.39 ± 0.04	0.39 ± 0.01
S4	0.35 ± 0.04	0.39 ± 0.01
S5 (Intermediate asymmetry)	0.35 ± 0.06	0.41 ± 0.02
S7 (Minimum asymmetry)	0.43 ± 0.05	0.47 ± 0.01
S8 (Minimum asymmetry)	0.42 ± 0.06	0.46 ± 0.01
Simulation results from literature	Surfactant-cosurfactant, BTMAC-SA (gel), ∼0.4[a,b] Lipid, DMPC (gel-ripple), ∼0.3-0.45[b] Cationic surfactant, DIDMAS-AHT (ripple), ∼0.39[c]	
Experiment results from literature	Lipid, DPPC (gel) ∼0.5[d]	

B_0 is a fitting parameter and R is the universal gas constant. This means that lower the P_2 having higher disorder in surfactant chains, higher is the configurational entropy per chain. Since measurement of entropy of lipid chains are challenging experimentally, measuring order-parameter can be an alternate probe to access per chain entropy using the above empirical relation. Similar relation is valid for conformational entropy of side chains of the proteins and the respective order parameter from NMR experiments [Li and Brüschweiler, 2009; Sapienza and Lee, 2010]. Moreover, the dependence of bilayer thickness, interdigitation, order parameter on per chain configurational

Table 4.7: Average order parameter, P_2 of simulated bilayers at AA and CG resolutions.

System	AA		CG	
	BTMAC	SA	BTMAC	SA
S1 (Maximum asymmetry)	0.68 ± 0.021	0.72 ± 0.006	0.82 ± 0.026	0.91 ± 0.005
S2 (Maximum asymmetry)	0.88 ± 0.008	0.89 ± 0.002	0.90 ± 0.016	0.91 ± 0.001
S3	0.83 ± 0.007	0.80 ± 0.006	0.91 ± 0.022	0.88 ± 0.002
S4	0.75 ± 0.002	0.79 ± 0.004	0.92 ± 0.045	0.98 ± 0.001
S5 (Intermediate asymmetry)	0.78 ± 0.031	0.85 ± 0.008	0.89 ± 0.027	0.93 ± 0.004
S6 (Intermediate asymmetry)	-	-	0.89 ± 0.026	0.93 ± 0.004
S7 (Minimum asymmetry)	0.92 ± 0.013	0.96 ± 0.004	0.93 ± 0.035	0.98 ± 0.002
S8 (Minimum asymmetry)	0.92 ± 0.024	0.96 ± 0.002	0.92 ± 0.02	0.95 ± 0.002
Simulation results from literature	Lipid (CG), DPPC (gel) ∼0.87 [Wang *et al.*, 2016c]			

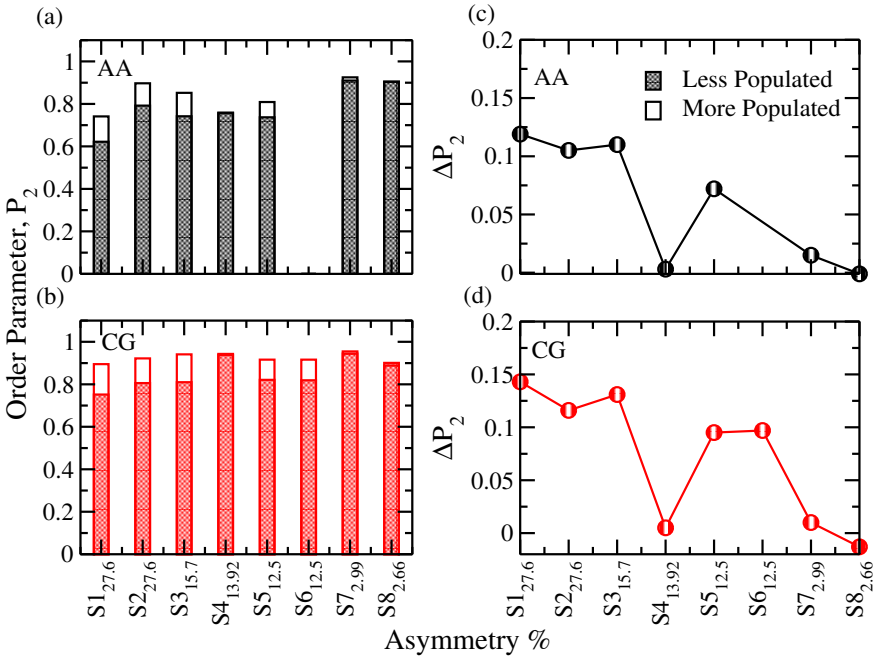

Figure 4.20: Order parameters, P_2, for two monolayers for all the systems in (a) AA and (b) CG resolution. P_2 across two layers are shown in same location to describe the difference in P_2 between the two leaflets. (c) and (d) show the differences in order parameters (ΔP_2 with respect to asymmetry percentage at AA and CG levels respectively.

entropy indicate that the integrated information from these physical properties can be crucial to determine entropy per chain of the asymmetric bilayers. The limitations of the per chain entropy calculations are not expected to affect these dependencies as changes in per chain entropy with respect to these parameters are more important than their absolute values. The effects due to quasi-harmonicity and correlated motions on the absolute values of per chain entropies should be scaled equivalently for all cases and should not have any significance for these calculations.

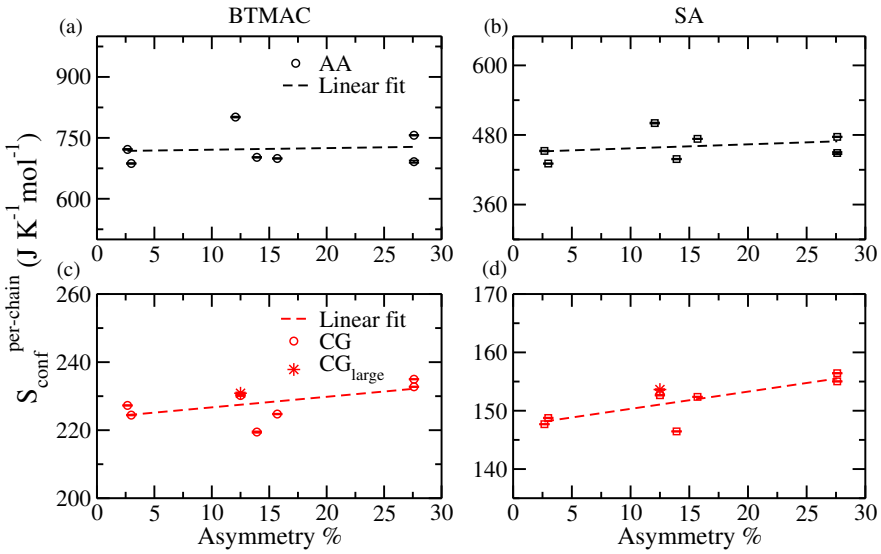

Figure 4.21: Variation of per chain configurational entropy with asymmetry at AA resolution: (a) BTMAC, (b) SA and CG resolution: (c) BTMAC, (d) SA. The data point shown in star: S6 bilayer with larger system size. $S_{conf}^{per-chain}$ increases with increasing asymmetry percentage. The error bar represents the standard deviation around time-frames over which $S_{conf}^{per-chain}$ converged and over all molecules.

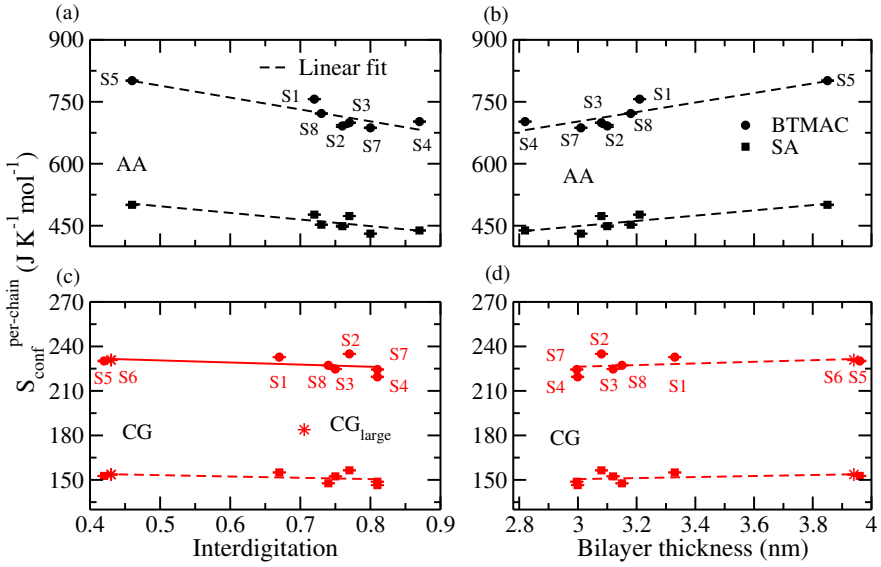

Figure 4.22: Variation of per chain configurational entropy with bilayer thickness (a)-(b) and interdigitation (c)-(d). Black: AA, red: CG. The data point shown in star: S6 bilayer with larger system size. $S_{conf}^{per-chain}$ increases with bilayer thickness and decreases with interdigitation. The error bar represents the standard deviation around time-frames over which $S_{conf}^{per-chain}$ converged and over all molecules.

4.5 SUMMARY AND CONCLUSIONS

Subsequent all-atom and coarse-grained MD simulations are employed using total 45.38 μs run-lengths to investigate the effect of trans-leaflet asymmetry on the stability and lateral

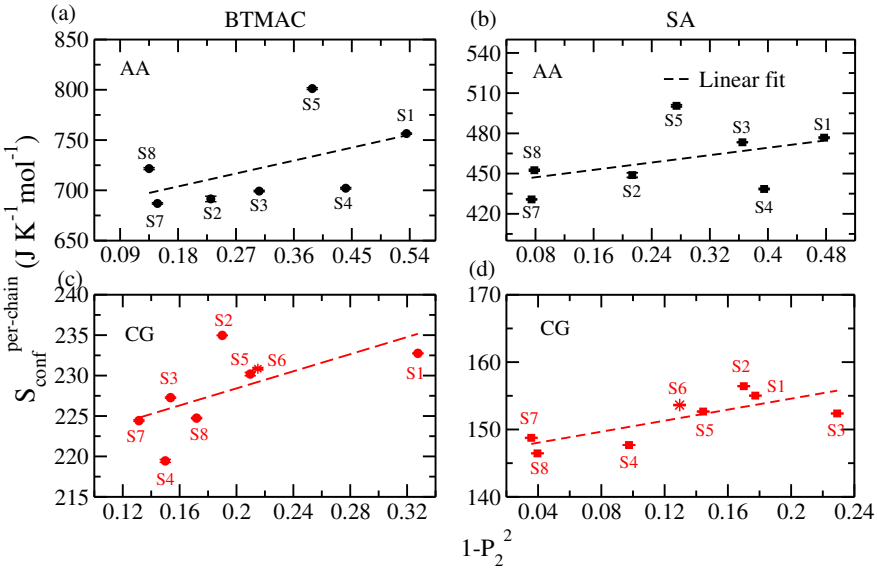

Figure 4.23: Variation of per chain configurational entropy with $(1 - P_2^2)$ at AA resolution: (a) BTMAC, (b) SA and CG resolution: (c) BTMAC, (d) SA. The data point shown in star: S6 bilayer with larger system size. The error bar represents the standard deviation around time-frames over which $S_{conf}^{per-chain}$ converged and over all molecules.

organizations of bilayers at gel/1D/2D ripple phases. Intertwining behavior of asymmetry with per chain entropy and interdigitation are analyzed towards inducing a rippled phase. Spontaneous self-assemblies of bilayers comprised of BTMAC and SA at a ratio of 2:1 result in asymmetric and interdigitated bilayers at 283 K starting from various random initial configurations in AA simulations. Since mixed surfactant molecules may not have spontaneous homogeneous self-assembly across two leaflets, an AA simulation is carried out starting from a symmetric configuration which too transforms into an asymmetric rippled bilayer.

The difference in the total number of BTMAC and SA molecules across two leaflets is referred to as asymmetry in the current study. A non-uniform variation in asymmetry percentage is observed within the systems simulated due to the unbiased spontaneous nature of the self-assembly processes. Most bilayers with the same ratio of BTMAC to SA at the same temperature starting with biased or random initial configurations result in an 1D or 2D rippled phase if the asymmetry percentage is higher. The ripple phases remain stable till room temperature by keeping asymmetry intact. To capture a longer length and time scale more relevant for examining the stability, a CG model is developed. The bonded potentials are obtained from Boltzmann inversion of the respective canonical sampling. The non-bonded potentials are obtained from the MARTINI force-field. Similar methodology of coarse-graining with an assumption of independent bonded and non-bonded potentials have been successfully implemented for polymers, lipid bilayers, liquid crystals, proteins in membranes and so on [Bezkorovaynaya *et al.*, 2012; Tschöp *et al.*, 1998; Debnath *et al.*, 2015]. Our CG model utilizes a scheme of separation of variables followed by derivations of bonded potentials which are implemented within the MARTINI framework to study mixed surfactant asymmetric bilayers. Similar to our approach, Lennard Jones interactions are used in place of harmonic bonds in the ELNEDIN protein model within the MARTINI framework for developing CG models of protein unfolding [Poma *et al.*, 2017b]. Structure based coarse-grained models have earlier been developed to study deformations of polysaccharides such as cellulose and β-amyloid [Poma *et al.*, 2017a]. All CG distributions of bonds and angles of both BTMAC and SA are found to be in good agreement with the respective AA distributions. The CG density profiles of both BTMAC and SA in all systems match reasonably well with their respective AA profiles reproducing the AA interdigitation. The interdigitation, thickness, tilt of the AA rippled bilayers are reproduced

well in the CG simulations. Although MARTINI does not generally reproduce ripple phase, tuning bonded potentials in combination of MARTINI non-bonded potentials can be suitable to obtain an interdigitated asymmetric lamellar gel or ripple phase. Moreover, these results validate our assumptions of independent bonded and non-bonded interactions in deriving the CG model for the mixed surfactant systems similar to single component system [Rühle *et al.*, 2009].

The density profiles of the opposing leaflets confirm the presence of two differently populated monolayers generating the asymmetry in all bilayers in both levels of resolutions. Two classes of molecules, ordered and disordered with distinct per chain configurational entropy are found for all AA bilayers. The less populated layer is found to have more disordered molecules with higher per chain configurational entropies for all systems. The inhomogeneity in distribution of disordered molecules across two leaflets decreases as asymmetry decreases. Two monolayers in the maximum asymmetric bilayer have different order parameters and the difference reduces as the asymmetry in composition reduces at both levels of resolutions.

In our simulations, three situations are identified in stabilizing the asymmetric bilayers. 1) Inhomogeneities in populations of disordered molecules (with higher per chain entropy and higher tilt) across two leaflets in a bilayer cause curvature in the system which leads to the formation of 1D/2D rippled bilayers (S1 to S6 except S4). The disordered molecules stay within micro-domains of the less populated layer. This causes a localized weak packing across leaflets with less interdigitation and phase asymmetry in the system. This localized larger thickness domains create larger hydrophobic barrier for a molecule to tumble up. Next to these disordered micro-domains, ordered molecules from both layers interdigitate strongly and flip-flop is inhibited and the asymmetry remains intact. AA-MD study conducted on zwitterionic DMPC membranes has shown that a large number of flip-flop events are coupled to spontaneous pore formation and the flip-flops are carried out by thermal fluctuations [Gurtovenko and Vattulainen, 2007]. In the current work, trans-membrane tumbling of very few surfactant molecules are only observed during an initial period of AA simulations when the symmetric bilayer transforms into an asymmetric rippled bilayer (S5). This clearly suggests that very few flip-flops of BTMAC/SA across the midplane of the interdigitated rippled domain occur by the thermal fluctuations to get rid of the local instabilities induced by the symmetry in the mixed surfactant bilayer system. Trans-membrane flip-flop is not found to be essential to maintain the stability of the bilayer once bending is achieved in the mixed surfactant bilayer systems unlike other bilayers [Boon and Smith, 2002; Karin *et al.*, 2002]. 2) There exists another asymmetric bilayer at gel phase with tilt symmetry and strong interdigitation across two leaflets (S4). The asymmetry is facilitated via complementary area per head group expansion across two leaflets. 3) Systems with minimum asymmetry (S7 & S8) show strong packing, least tilt and phase symmetry across two leaflets. Thus the chains in such bilayers are again strongly interdigitated resulting in a gel phase. Hence, the asymmetry in disordered chains with higher per chain configurational entropy and tilt maintain ripple phase intact in the mixed surfactant bilayers.

Thus our calculations provide molecular insights on the lateral organizations of 1D ripple or square phase induced by trans-leaflet asymmetry for a mixed surfactant system where relevant length and time scales are captured using the multi-scale simulation ansatz. A transition of the gel phase to the 2D/1D rippled phase can be achieved by increasing populations of disordered molecules across leaflets without varying temperatures and concentrations. Previous simulations using MARTINI model shows that asymmetry is not important to generate vesicles at gel phase where the kinetic barrier of the effective area constraint of lipids are overcome by introducing artificial pores [Risselada and Marrink, 2009]. Earlier, different replicates of pure DMPC bilayer have generated both gel and rippled phases at 275.15 K using atomistic simulations [Khakbaz and Klauda, 2018]. Thus asymmetry percentage can act as a controlling parameter to obtain industry and pharmaceutically relevant desirable phases at same temperature and concentration.

Bilayer properties such as order-parameter, bilayer thickness and interdigitation have linear dependence on per chain configurational entropy which is again dependent on asymmetry. Since

configurational entropy of surfactant chains in an asymmetric bilayer is difficult to obtain through experiments, the structural properties of the asymmetric bilayer can serve as a proxy to derive the configurational entropy at both levels of resolutions. In a similar line, NMR-based generalized order parameter is reported to work as a monitor for the inaccessible conformational entropy of protein side chains [Kasinath *et al.*, 2013]. Our results predict that the NMR techniques can be used to derive generalized order parameter of surfactant molecules to monitor the entropy per chain for bilayers. The understanding of asymmetry induced gel to ripple phase transition in a surfactant bilayer can be extended and tested to study asymmetric membranes in fluid phase. Moreover, disordered domains in the square phase can nucleate pore formation or enhanced permeability across bilayers. This can open up a new avenue to find out the influence of configurational entropy in determining the free energy of asymmetry which is crucial in poration of asymmetric cell membranes at low temperature.

Publication: **Arpita Srivastava** and Ananya Debnath, Asymmetry and rippling in mixed surfactant bilayers from all-atom and coarse-grained simulations: Interdigitation and per chain entropy **2020**, Journal of Physical Chemistry B, *124*, 6420.